Performance prediction and fault diagnosis of an axial piston pump under different leakage conditions

MS (Research) Thesis

By

RISHABH GUPTA

DEPARTMENT OF MECHANICAL ENGINEERING

INDIAN INSTITUTE OF TECHNOLOGY INDORE

MAY, 2022

Performance prediction and fault diagnosis of an axial piston pump under different leakage conditions

A THESIS

Submitted in fulfillment of the

requirements for the award of the degree

of

Master of Science (Research)

By

RISHABH GUPTA

DEPARTMENT OF MECHANICAL ENGINEERING

INDIAN INSTITUTE OF TECHNOLOGY INDORE

MAY 2022

INDIAN INSTITUTE OF TECHNOLOGY INDORE

CANDIDATE'S DECLARATION

I hereby certify that the work which is being presented in the thesis entitled **Performance prediction and fault diagnosis of an axial piston pump under different leakage conditions** in the fulfillment of the requirements for the award of the degree of **MASTER OF SCIENCE (RESEARCH)** and submitted in the **DEPARTMENT OF MECHANICAL ENGINEERING, Indian Institute of Technology Indore,** is an authentic record of my own work carried out during the time period from August 2020 to May 2022 under the supervision of **Dr. Pavan Kumar Kankar,** Associate Professor in Mechanical Engineering, Indian Institute of Technology Indore.

The matter presented in this thesis has not been submitted by me for the award of any other degree of this or any other institute.

Rishabh 30/05/2022
Rishabh Gupta
(Student)

This is to certify that the above statement made by the candidate is correct to the best of my/our knowledge.

30/05/22
Dr. Pavan Kumar Kankar
(Thesis Supervisor)

Rishabh Gupta has successfully given his MS (Research) Oral Examination held on 10 August 2022.

10/8/2022
Signature of Chairperson (OEB) with date

10.08.2022
Signature(s) of Thesis Supervisor(s) with date

10/8/2022
Signature of Convener, DPGC with date

10.08.2022
Signature of Head of Discipline with date

ACKNOWLEDGEMENTS

Above all, I'd want to thank God for the life experiences, accomplishments, and failures that have shaped me into the person I am today. My heartfelt gratitude goes to my parents and brother for their love, sensitivity, and faith in me.

The entire MS (Research) program has been a valuable experience for me, not only in terms of acquiring skills in the fields of **condition monitoring, fluid power, hydraulics, simulations, and control system**, but also in terms of learning a lot more about methods, research, work attitudes, and interpersonal relationships.

I thank my supervisor, **Dr. Pavan Kumar Kankar**, for motivational support. Thanks for providing me an opportunity to work at the System Dynamics Lab (SDL), IIT Indore, and giving me valuable suggestions to improve and take ownership of my work. I also thank faculty members who were part of my MS (Research) PSPC committee members: **Dr. Ankur Miglani** and **Dr. Sandeep Chaudhary.** Your sincere and personal interest in me, professional attitude, and guidance concerning my work and project have allowed me to work with a clear mind and a free heart. To me, you have been an outstanding teacher, mentor, and role model, and I have learned a lot from you all.

I also want to thank **Mr. Shyam Zambre** (DGM, Volvo Eicher commercial vehicle Pvt. Ltd) for giving me practical exposure to the uptime center, industrial aspects, and live monitoring of on-road commercial vehicles.

My life as an M.S. (Research) student at IIT Indore would not have been the same without my classmates. Everyday activities, politically incorrect jokes, informal fikas that may go for hours, and, probably most significantly, our frequent after-works help make our division the greatest at IIT Indore. This thesis would not be possible without the unending support of my parents, who have helped me get to where I am now. My gratitude also extends to all lab colleagues, whose assistance has been priceless and has made working in the lab one of the most appealing aspects of my MS (Research) studies. It's a joy to collaborate with them.

Thanks a lot, everyone...!

RISHABH GUPTA

Dedicated to my family for their love, care, and blessings…!

Abstract

In axial piston pumps (APP), the leakage fault can degrade the pump's performance and limit its predictability and reliability. As a result, APP condition monitoring can be used for preventative maintenance and for selecting the most effective methods to reduce operating costs and improve performance. The Leakage is modelled as laminar flow past the uniform annular gap between the piston and cylinder. With a single faulty cylinder, as the wear (annular gap) increases, the pump's time-mean outlet flow and pressure remain constant until a critical threshold and then reduce rapidly, leading to deterioration in the pump's volumetric efficiency. With the increase in faulty cylinders, this critical threshold shifts to lower magnitudes, and in the limit of more than four faulty cylinders, this threshold saturates to a constant magnitude. In this research, the dynamic signal data show that the increasing severity of leakage and an increasing number of faulty cylinders modulate both the time signature and the amplitude fluctuations of the outlet pressure waveform due to the reduced flow in the discharge cycle. Further, FFT analysis of these dynamic signals and the time-mean value of pressure and flow rate leakage fault diagnosis is presented to classify the pump's condition as either healthy, moderately faulty, or severely faulty.

Further, a simulation and mathematical model-based approach are presented to simulate the effect of increasing severity of leakage fault (increasing annular gap) in single and multiple cylinders simultaneously on the pump performance. Moreover, when using an APP, there is a possibility of wear (internal leakage) occurring in multiple pistons-cylinders simultaneously. In the event of multiple pistons failing, inline arrangements are the ideal but not best configuration layout of defective pistons for mitigating peak-to-peak fluctuations during pump discharge. In such faulty pump conditions, the pressure and flow variation create vibrations, which can cause premature failure of pump components. So, when it comes to finding out which configuration of defective pistons would result in the lowest peak-to-

peak pressure variations under internal leakage at APP's outlet, a model simulation and analytical technique have been proposed.

Moreover, it was also discovered that the amplitude waveforms of dynamic signals changed in response to each leakage fault (20 μm, 60 μm, and 100 μm), which helped to visualize the growing severity of a leakage fault (h) as well as the various potential configurations for defective pistons (N), respectively. A dynamic pressure/flow data study is used to categorize the pump's condition as either worst-case, somewhat intermediate, or best-case for the respective number of defective piston configurations (N) corresponding to various leakage severities (h).

LIST OF PUBLICATIONS

❖ **Book Chapter**

1. **Rishabh Gupta**, A. Miglani, P. Kankar. On the validity of parallel plate assumption in modelling leakage fault in hydraulic actuators, in Intelligent Prognostics for Engineering Systems with Machine Learning Techniques. *CRC Press, Taylor and Francis, (2021). (**Accepted**)*

❖ **International Journal Articles**

1. **Rishabh Gupta**, Ankur Miglani and Pavan Kumar Kankar; "Performance prediction of an axial piston pump with increasing severity of leakage fault in single and multiple cylinders, *ASME J. of Systems, Measurement, and Control*, ***in review*** (2021).

2. **Rishabh Gupta,** Ankur Miglani and Pavan Kumar Kankar; " Mitigating pressure fluctuations of a faulty axial piston pump by rearranging pistons", *Proceedings of the Institution of Mechanical Engineers, Part C,* ***in review*** (2022).

❖ **Patent**

1. Inventors: **Rishabh Gupta**, A. Miglani, P. Kankar. Patentee: IIT Indore. A method for increasing the utilization of an axial piston pump under leakage fault conditions ***Complete Patent with First Examination Report (FER) filed*** (2022).

TABLE OF CONTENTS

LIST OF FIGURES	**xiii**
LIST OF TABLES	**xvii**
NOMENCLATURE	**xix**
ACRONYMS	**xxiii**

Chapter 1: Introduction	**1**
1.1. Background: Description of axial piston pump	1
1.2. Applications	2
1.3. Working	3
1.4. Different faults and causes in axial piston-pump	3
1.5. Thesis outline	5
Chapter 2: Literature review	**7**
2.1. Introduction	7
2.2. Previous literature: Piston-cylinder leakage fault in APP	7
2.3. Research objectives	11
Chapter 3: Mathematical modelling: axial piston pump	**13**
3.1. Introduction	13
3.2. Assumptions	13
3.3. The mathematical annular leakage flow model	14

3.4. Mathematical model for Pump's discharge pressure/flow 18
3.5. Model for the load condition 21
3.6. Summary 21

Chapter 4: Simulation: Leakage conditions in APP 23

4.1. Introduction 23
4.2. Simulation-modelling approach and method--ology 23
4.3. Parameters used for simulating/mimic axial piston pump 24
4.4. APP's control System network model 26
4.4.1. Model for the closed-loop hydraulic circuit 26
4.4.2. Model for the axial piston pump 27
4.4.3. Model of a single piston-cylinder assembly 28
4.5. Model Validation 29
4.5.1. Parameters for model validation 29
4.5.2. Comparison between model and experimental studies 31
4.6. Summary 33

Chapter 5: Leakage fault severity in single and multiple cylinders 35

5.1 Introduction 35
5.2. Results and Discussion 36
5.2.1. Dynamic signals response analysis 36
5.2.1.1. Leakage fault signals in a single cylinder 39

5.2.1.2. Leakage fault signals in multiple cylinders 43
5.2.2. Time-mean response analysis 46
5.2.3. APP's health detection through FFT analysis 49
5.2.3.1. Single cylinder fault detection 49
5.2.3.2. Multiple cylinder's fault detection 53
5.3. Summary 54

Chapter 6: Arrangement of faulty pistons 57

6.1. Introduction 57
6.2. Methodology 58
6.3. Arrangements 60
6.4. Results and Discussion 62
6.5. Summary 68

Chapter 7: Conclusions and Scope for Future Work 69

7.1. Introduction 69
7.2. Research conclusion: Leakage fault severity in single and multiple cylinders 69
7.3. Research conclusion: Arrangement of faulty piston 71
7.4. Recommendations for future work 73

APPENDIX-A: Derivation of configuration ratio (CR) 75

REFERENCES 77

LIST OF FIGURES

Fig. 1.1	Schematic exploded view of the axial piston pump with important geometric parameters are shown marked.	**1**
Fig. 3.1	Schematic of the axial piston pump: cross-sectional view through the center plane (right), sectional view along the plane A-A' (left).	**14**
Fig. 3.2	a) Sectional view of the piston-cylinder arrangement showing the oil leakage path through a uniform annulus of width h. b) In-depth annular leakage flow path and velocity profile.	**15**
Fig. 3.3	Schematic representation of a few selective leakage fault cases investigated in this study: (a) cross-sectional view of the piston-cylinder arrangement showing increasing severity of leakage fault in a single cylinder, and (b) the complete cylinder block with leakage fault in multiple cylinders simultaneously; three faulty cylinders (1, 2 and 3: in red colour), and six healthy cylinders (4 – 9: in green colour).	**15**
Fig. 4.1	Block model of the hydraulic system network for simulation of leakage fault in an axial piston pump with different degree of wear in single and multiple cylinders.	**24**
Fig. 4.2	Simscape block model of an axial piston pump with nine pistons.	**28**
Fig. 4.3	Simscape block model of a single piston-cylinder assembly with the interfacing mechanical linkages, hydraulic lines, signal lines and flow and pressure sensors.	**29**
Fig. 4.4	Dynamic pressure signal (at APP output conditions 2, 5, and 10 Mpa) comparison between the current study's model predictions	**32**

(solid line) and the experimental data (dotted line) of Ref. [9] for a single-cylinder (top) and at the pump outlet (bottom).

Fig. 4.5 Comparison of dynamic pressure signal between the model-predictions (solid line) of the current study and the experimental results (dotted line) of Ref. [10] for a single cylinder (top), and at the pump outlet (bottom). **33**

Fig. 5.1 Schematics for cylinder's cross-sectional view with N = (1 to 9) numbers of faulty piston-cylinder in axial piston pump. **36**

Fig. 5.2 Dynamic response signals of individual cylinders and their net output at the pump discharge for a single faulty cylinder (left), and multiple faulty cylinders (right: representative for two faulty cylinders). The leakage fault severity for both cases is h= 60 µm. The top and bottom rows represent the temporal variation of flow rate and pressure, respectively. **38**

Fig.5.3 Dynamic pressure signal at the pump outlet at different degrees of leakage fault: (Top) for one pumping cycle. (Bottom) for three pumping cycles. **41**

Fig. 5.4 Temporal variation of the net pressure at the pump outlet over one pumping cycle. The pressure-decay, pressure-build-up and pressure restoration for two faulty conditions (h= 60 µm and 80 µm) are shown marked. **42**

Fig. 5.5 Temporal variation of the net pressure at the pump outlet with increasing number of faulty cylinders, at different levels of fault severity: (a) $h = 1$ µm, (b) $h = 30$ µm, (c) $h = 40$ µm, (d) $h = 50$ µm, (e) $h = 60$ µm, and (f) $h = 80$ µm. **45**

Fig. 5.6	Time-mean response of (a) flow rate, and (b) pressure at the pump outlet as a function of severity of leakage fault and the number of faulty cylinders.	**48**
Fig. 5.7	FFT spectra at different levels of leakage fault severity: (a) $h = 1$ µm, (b) $h = 10$ µm, (c) $h = 30$ µm, (d) $h = 40$ µm, (e) $h = 50$ µm, (f) $h = 60$ µm, (g) $h = 80$ µm, and (h) $h = 100$ µm.	**52**
Fig. 5.8	Variation of the parameters R_1 (Eq. 26) and R_2 (Eq. 27) with the severity of leakage fault.	**54**
Fig. 6.1	Applied methodology to evaluate the configuration of the piston.	**58**
Fig. 6.2	Exploded view of axial piston pump (APP), followed by subdivision of piston arrangements such as: All healthy, inline, random, uniform, and all defective respectively for pistons fault severity of $N = 3$.	**59**
Fig. 6.3	Illustrates all possible geometrical arrangements of faulty pistons classification under the different levels of piston faults severity $N \in$ [1-9].	**61**
Fig. 6.4	Plots for a peak-to-peak amplitude for the respective number of piston faults corresponds to different (worst (W), intermediate (R) and best (B) cases); (a) h =20 µm, (b) h =60 µm, (c) h =100 µm.	**64**
Fig. 6.5	Temporal variation of the net pressure at the pump outlet with the number of faulty Pistons; $N = 2$ **(a-c)** at different levels of leakage severity: h = 20, 60 and 100 μm respectively.	**66**
Fig. 7.1	Variation of volumetric efficiency of pump with increasing severity of leakage fault and number of faulty cylinders.	**70**
Fig. A.1	Cross-sectional view of cylinder barrel of APP with all 9 pistons arrangements. Each vertex of the triangle is considered the center of a	**76**

piston; $\boldsymbol{P_1}$ $\boldsymbol{to}$ $\boldsymbol{P_9}$ Coordinates (X, Y) respectively, and **O** (0,0) act as a center of origin of whole circular geometry.

LIST OF TABLES

Table 1.1	Numerous sorts of defects and their causes in various regions of Axial piston pump (Vickers Variable Displacement Axial Piston Pump PVB 5**).**	**3**
Table 3.1	Phase angle and position of the pistons at the initial condition ($t = 0$ s).	**19**
Table 4.1	System parameters used for simulating leakage fault in an axial piston pump.	**25**
Table 4.2	Parameters reported in Ref. [10] and used as model inputs for validation.	**30**
Table 5.1	The range of fault severity that determine the pump's condition corresponding to the number of faulty cylinders. Note that the range of fault severity for moderately faulty conditions reduces with increasing number of faulty cylinders and vanishes for five or more faulty cylinders.	**47**
Table 6.1	Theoretical value of CR $(\emptyset)$ corresponds to the value of each N and pistons arrangements.	**62**

NOMENCLATURE

Symbols

R	radius (m)
P	pressure (Pa)
R_c	radius of cylinder (m)
R_p	radius of piston (m)
D_p	diameter of piston (m)
D_d	cylinder orifice diameter (m)
H	width of annular gap (leakage gap: $R_c - R_p$) (m)
$X_{(pi)_i}$	initial position of i^{th} piston (m)
x_a	initial position at t = 0 (m)
X_{pi}	piston displacement/stroke of i^{th} in x-direction (m)
V_{pi}	piston velocity of i^{th} in x-direction (m/s)
a_{pi}	piston acceleration of i^{th} in x-direction (m^2/s)
r_{pitch}	cylinder pitch radius (m)
r_a	radius of the actuator arm (m)
S_p	piston stroke (m)
$Q_{net,k}$	net kinematic flow rate at pump discharge (m^3/s)
$Q_{pc_{net}}$	total flow rate to discharge chamber (m^3/s)
Q_{kp}	kinematic flow rate delivered by the piston (m^3/s)
$(Q_{pc})_i$	flow rate from $i^{th} -$piston to the pump discharge chamber (m^3/s)
$Q_{leakage}$	leakage flow past the piston-cylinder annulus gap (m^3/s)
Q_{out}	net flow rate at pump outlet (m^3/s)
$P_{pc,i}$	i^{th} - cylinder chamber pressure (Pa)
P_{pi}	instantaneous pressure of cylinder chamber (Pa)

P_{out}	pump output pressure (Pa)
$V_{c,i}$	initial clearance volume of a cylinder (m^3)
V_{dead}	fixed dead volume (m^3)
V_{Ch}	volume of pump discharge chamber (m^3)
C_d	coefficient of discharge (-)
A_d	area of cylinder discharge orifice (m^2)
A_p	cross-sectional area of piston (m^2)
A_{load}	area of constant load orifice (m^2)
K_b	bulk modulus of the fluid (Pa)
T	temperature (°C)
Re_{cr}	critical reynolds number
X	pump rotational frequency (Hz)
f	pump discharge frequency (Hz)
T	time (s)
v	kinematic viscosity
R_1 , R_2	ratios of amplitudes of the pump's discharge frequency to the amplitude of its sideband frequencies

Greek letters

μ	dynamic viscosity (N-s/m^2)
γ	phase angle of suction valve plate (degree)
α	swash plate angle (degree)
θ	angular position (degree)
ω	angular velocity of the drive shaft (rad/s)
ω_p	angular velocity of pistons ($=\omega$: rad/s)
$\dot{\omega}_p$	angular acceleration of pistons (rad/s^2)
δ	phase delay angle between cylinders (degree)

ρ_{fluid} , ρ_{air}	fluid and air density (kg/m^3)
ϵ	ratio of amplitudes of pump rotational frequency and discharge frequency

Subscripts

k	kinematic
i	cylinder index
net	resultant flow parameter (flow rate or pressure)

ACRONYMS

APP	axial piston pump
CR	Configuration ratio
FFT	Fast Fourier Transform

Chapter 1

Introduction

1.1. Background: Description of axial piston pump

Axial piston pumps (APP) or simply swash plate pumps (fixed or variable displacement) are widely used in aerospace, shipping, automobile, and construction machinery due to their high-pressure ratings, high force-to-weight ratio, and ability to utilize fluids under pressure to transmit power. For efficient operation, the APPs are manufactured to fine tolerances between the mating faces of the piston-cylinder assembly, which enable sufficient lubrication between the sliding faces while maintaining a tight seal even at high rotational speeds (~3000 rpm). While their robust design makes them one of the most efficient types of pumps with excellent pressure rating (as high as ~ 650 bar) [1], they are highly prone to wear by contaminants. APPs involve relative motion between many components running under tight tolerances; for instance, the piston bore clearance is ~10 - 12 µm [2-3] in a new APP.

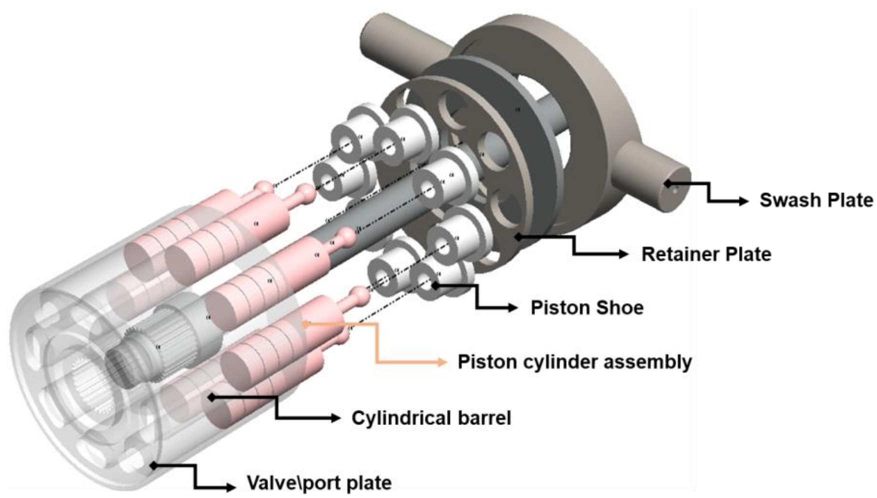

Fig. 1.1: Schematic exploded view of the axial piston pump with important geometric parameters are shown marked.

1.2. Applications

Piston pumps are not broadly applicable but specialists in specific tasks: When the environment is harsh or the pressure rises to extreme levels, these tough machines thrive. These pumps can handle conveying pressures of up to several thousand bar depending on the design. Piston pumps have a wide range of uses and may transport both liquids and gases. These robust devices come in various sizes and perform safely and reliably even in tough environments. These pumps are utilized in the industrial sector with a high conveying pressure.

- Chemical industry
- Oil & gas
- Automobile and defense
- Energy management
- Water & wastewater treatment
- Steel & rolling mills
- Galvanizing & ceramic shops

Piston pumps can perform the job where other pumps fail, whether in the chemical sector, transporting and processing oil and gas, or mining and wastewater treatment. With sophisticated pulsation compensation equipment and subsequent advances such as diaphragm technology, these units that have established themselves over centuries indicate on a daily basis that their evolution is far from done; instead, they can always be changed to meet the needs of users. Are diverse as the sectors in which they are utilized, and as many as the conceivable uses of piston pumps, a full list is difficult to compile.

1.3. Working

Positive displacement pumps, unlike centrifugal and other rotatory pumps, do not employ centrifugal force; instead, they actively displace liquids — with the piston for which they are called. By a stroke movement, this piston is fed directly into a cylinder; the cylinder is sealed with a valve at the intake and output. The piston travels out of the pump housing during the suction phase, opening the intake valve and allowing liquid to flow into the cylinder. The conveying action causes the piston to return to the housing, the outlet valve to open, and the medium to exit the pump.

1.4. Different faults and causes in axial piston pump

Figure 1.1 shows a variable displacement axial piston pump with a swash plate, valve/port plate, slipper, barrel, driving shaft, multiple pistons, and bearings, among other components. Each component of the pump is prone to wear and, if not diagnosed early, can lead to catastrophic failure. As illustrated in Table 1.1, there are numerous defects and their causes in various regions of APP, which significantly reduce pump performance. However, the primary focus of this study is solely on piston-cylinder leakage faults (1st row in table 1) circumstances corresponding to single and multiple cylinders.

Table 1.1: Numerous sorts of defects and their causes in various regions of Axial piston pump

Components	Causes (Faults)	Effects
1. Piston	Wear (Internal leakage increased)	▪ Bigger pressure ripple and flow waveform, ▪ Higher fluid & structural borne noises, ▪ Higher oil temperature, ▪ Insufficient suction vacuum,

		▪ Lower volumetric efficiency, ▪ Insufficient pressure generation.
2. Valve Plate	Wear (Friction increases, especially at the relieve groove and cavitation)	▪ High fluid borne noises, ▪ High leakage chance between the valve plate and barrel face, ▪ Lower efficiency, ▪ Increase oil temperature.
6. Retainer plate	Wear (Lack of lubrication and scoring)	▪ Broken retainer plate, ▪ Sudden breakdown of pump takes place, ▪ High noise and vibration.
4. Slipper	Pad and upper surface wear (friction increase)	▪ Non-uniform pressure ripple, ▪ High oil temperature, ▪ High structural borne noises, ▪ Lower volumetric efficiency.
5. Cylinder barrel	Wear (Lack of lubrication and pitting)	▪ High structural borne noises, ▪ Valve plate-barrel interface assembly wear, ▪ Non-uniform pressure ripple, ▪ Oil temperature near barrel opening ports increases faster, ▪ Lower efficiency.
6. Swash plate	Face wear (Friction increase)	▪ Increases oil temperature, ▪ Higher FBNs and SBNs, ▪ Required high on drive shaft, ▪ Lower efficiency.

1.5. Thesis outline

The sequence of the research procedure is developed in accordance with this thesis. It is divided into seven chapters, which are as follows:

Chapter 2. Literature review: Previous research on variable displacement axial piston pumps has used a variety of approaches and methodologies.

Chapter 3. Mathematical modelling: axial piston pump: Various assumptions and simplifications are considered in formulating the APP's Mathematical model.

Chapter 4. Simulation: 9-piston axial pump: A closed-loop flow network architecture of the APP's hydraulic control system involving a variable displacement axial piston pump is developed using Simscape; in the Simulink environment of MATLAB 2020b.

Chapter 5. Leakage fault severity in single and multiple cylinders: Analysis of the different degrees of leakage severity in single and multiple cylinders to understand the effect on the pump performance.

Chapter 6. Arrangement of faulty pistons: To demonstrate the methodology for analyzing the various piston-cylinder configuration layouts in this research and analyze the impact of piston configurations at different numbers of faulty pistons and leakage severity between the piston-cylinder (annular gap in microns) of an APP using the MATLAB-Simscape platform.

Chapter 7. Conclusion and Future work: The project's objectives are examined, as mentioned in Chapter 1. Significant findings have been established, and more study is recommended.

Chapter 2

Literature review

2.1 Introduction

This chapter highlights previous pivotal investigations into the severity of APP piston-cylinder leakage. Furthermore, substantial research gaps have been found through the literature material in this thesis, which can be easily understood by reading the current literature in the depth of this thesis. Finally, the study's research objectives can present the precise concept and essential results that will be highlighted throughout the thesis in subsequent chapters of this thesis.

2.2 Previous literature: Piston-cylinder leakage fault in APP

Leakage is the key performance-deteriorating effect of wear (and the resulting increase in clearances), and therefore, several prior studies [1 - 10] have focused on characterizing the effects of leakage. For instance, Tang et al. [6] presented a model-based method of leakage fault detection in ADAMS to investigate the dynamic response of an APP under different loading and structural health conditions. Their results showed that the outlet pressure signals are more responsive to a leakage fault than the signals of pump casing vibrations, and therefore, they are more suitable for detecting oil leakage faults. Furthermore, they investigated the response of pressure waveform at three levels of fault severity 5 μm, 100 μm and 200 μm, and four levels of external load (5, 10, 15 and 23.5 MPa) and showed that the external load has a strong influence on the dynamic pressure signals in response to the oil leakage fault. Li et al. [7] developed a Simscape model to simulate the oil leakage fault in a single cylinder and demonstrated that oil leakage fault causes a concave dip in the pressure waveform, increasing fault severity. Kumar et al. [8] updated the model of Ref. [7] and, through simulations in the simscape platform, demonstrated that the deviation in pressure waveform resulting from the leakage fault can be corrected to within the permissible levels using a PID controller. Zhang et al. [9] developed a seven-stage model for predicting the oil film thickness between the valve plate and cylinder block in an axial piston pump under wear conditions at different pump load and rotational speeds, which is crucial for ascertaining the pump's health. Bergada et al. [10] developed an analytical model to decipher the effect of flow loss across multiple gaps in piston pump (slipper/swash plate, barrel/valve plate and piston/cylinder bore) on the resulting flow/pressure dynamics and validated their results against the existing numerical models. As APPs have become increasingly complex in construction and offer diverse functionalities due to size, weight and performance demands, the use of scheduled maintenance for ascertaining their reliability is no longer a viable option. Instead, the reliability of an APP must be supported by condition monitoring (CM)-based maintenance schemes that are based on fault diagnosis. Such schemes will not only help in reducing unscheduled downtime by planning the maintenance but also aid in reducing operating costs by identifying the optimum working conditions. Several previous studies [11 – 22] have proposed condition monitoring approaches of fault detection in hydraulic systems, especially the APP's. For example, Yoder [14] developed a 1D physics-based model to simulate the hydrostatic bearing failure between the swash plate and slippers under different operating conditions, and subsequently proposed a health monitoring approach by tracking the changes the vibration signals. Chen, H. et al. [15] developed a dynamic model of the complete swash plate pump to obtain diagnostic information for distinguishing and evaluating the influence of defects in different components by capturing vibration signals from strategic locations in the pump body. Casoli et al. [16] also developed a vibration signal-based approach for detecting and classifying faults in hydraulic axial piston pumps. These extensive theoretical investigations are either based on signal-processing or machine learning-based methods, and despite their ability to identify faults and predict significant parametric trends of the fault growth, their implementation is limited due to some inherent limitations. For example, machine learning (ML)-based condition monitoring has an associated penalty in terms of its strong dependence on the quality of the training data set [17-19, 52]. It is well established that a large data set under different operational conditions (both healthy and faulty) is required to enable satisfactory training. However, the open literature lacks in experimental studies on APP and the data obtained from in practice operations is limited; due to the low failure probability of such high-safety and high-performance systems.

On the other hand, the fault feature extraction and noise removal using the signal-processing techniques rely heavily on measured responses, which are often complex and strongly influenced by the operational and external conditions [20]. Several Studies also showcased the novel methods such as three-piston pump design to test the different other components of axial piston pump [28]. Theoretical and simulative studies always possessed good results for validating the pump's dynamic and static characteristics with flow regulations and identifying the significant performance parameters by computer simulation [29]. System modeling comparison has been made through different simulation methods like AMESim and Adams simulation technique [30]. According to Manring et al. [31], the numerical findings of this study indicate that a pump with an even number of pistons may be as feasible as one with an odd number of pistons. Edge et al. [32] addressed a study of cylinder pressure and flow in an oil hydraulic axial piston pump, comparing a theoretical model based on fluid compliance within the cylinder to an upgraded model that accounts for the effect of oil impetus in the port plate region. Schoenau et al. [33] provide a fluid mechanics-based mathematical model of a variable displacement pump modulated by a hydraulic control signal. The research [34] presents closed-form equations that may be utilized to guide the conceptual model of a variable-displacement pump. The initial design of the control actuation system and the controller flow gain are both taken into consideration.

A dynamic model of the pumping system is also illustrated, as is the dynamic impact of parameter changes such as actuator volume, discharge-hose volume, controller flow gain, and system leakage. All these factors can significantly affect the reliability and accuracy of signal-processing and ML-based condition monitoring methods, thereby reducing their attractiveness for fault diagnosis. While oil leakage fault has been the focus of these investigations, the results therein have been limited to leakage fault is just one cylinder. In recent years, numerous academic research has investigated mainly about [31-32] pump dynamic of fluid flow, leakages [38-39], and noise and vibrations in a pump [42-44]. Interfacial behaviours including leakage, lubrication, friction, and temperature are also being studied [37], [44–48]. However, the potential of leaking in multiple piston cylinders and their optimized configurations are still absent. In the recent ten years, Ivantysynova et al. [37], [46–49] carried out a series of studies on the leakage of a swashplate pump, concentrating solely on the piston-cylinder contact.

All of these initiatives are assisting in improving the condition monitoring of piston pumps, but they are insufficient for improving APP downtime and maintenance practices. Furthermore, these studies considered the effect of faulty severity based on arbitrarily chosen values of the annular clearance and based on these arbitrary values the leakage faults were designated as normal, slight, or severe. Instead of using conventional condition monitoring methods based on observing the variation tendencies of the fault features (signal processing) over time, a more effective and reliable troubleshoot method (demonstrated in this paper) that increases the downtime and performance of the axial pump is required to implement for the faulty piston-cylinders inside the APP.

2.3 Research objectives

In an axial piston pump, the wear or failure may occur not in just one part but several parts simultaneously, which may change the operating parameters and rapidly deteriorate the pump performance. For instance, in a system with multiple cylinders, the wear (and hence the leakage) in one or more cylinders will lead to non-uniform delivery at the pump outlet and the downstream fluid power system. As the worn-out cylinders deliver reduced flow relative to the healthy ones, it may trigger undesirable aperiodic flow fluctuations or result in transient pressure spikes. This can induce fatigue in pump components and cause premature failure, thereby limiting its performance prediction and the reliability of the overall system.

On the other hand, to the extended version of leakage severity in multiple piston cylinders, in an industrial setting, many situations may arise where a pump with an internal leakage fault is required to run for an extended period to meet the production demand. In this scenario, applying the best possible configuration of defective pistons onsite will allow the defective pump to run effectively to meet the demand pump's performance. This study also proposes a methodology for identifying the best (optimal) geometrical configurations of defective pistons resulting in minimum peak-to-peak pressure fluctuations at the outlet of an internally leaking APP. This method would allow the pump to operate at the least pressure fluctuations and vibrations at its outlet, furthermore by categorizing the various piston configurations based on their dynamics of net pressure responses using a model-based study. So, the Hydraulic industry can benefit from this technique in terms of cost and reusability of the pump.

The primary objectives of this proposed study can be followed as follows:

1. To develop a model-based technique for diagnosing a leaking problem between a piston-cylinder of a 9-axial piston pump, utilizing the

MATLAB-Simscape platform to mimic the real functional restrictions and operating circumstances of the APP presented.

2. To understand how the pump's performance is affected by the increasing severity of leakage fault in a single cylinder and multiple cylinders simultaneously.

3. By adopting various option configurations within a malfunctioning pump, a methodology for turning axial-piston pumps more efficient or flexible and reducing noise and downtime was developed.

4. Proposed approaches for repurposing defective pumps and extending their service life by reducing maintenance costs and simplifying operations can significantly improve the pump's reliability.

Chapter 3

Mathematical modelling: axial piston pump

3.1. Introduction

This chapter has developed a detailed mathematical model of a 9-piston axial pump and its piston-cylinder leakage equations, which mimic the APP's real functional constraints and operating conditions. In a subsequent part of this thesis, the mathematical model equations and constraints are applied to create a simulation model of APP. Based on the proposed mathematical equations for net flow/pressure and leakage conditions, the MATLAB-Simscape platform is utilized to directly evaluate the effects of leakage fault severity in single and multiple cylinders on the pump performance of an APP.

3.2. Assumptions

The following assumptions and simplifications are considered in formulating the APP’s Mathematical model:

1. The hydraulic fluid properties such as density, viscosity, and bulk modulus are temperature-independent and remain constant during pump operation.
2. Flow is laminar, and the fluid inertia is neglected.
3. Leakage is considered only via the annular gap between the piston and cylinder. All other flow losses such as slipper leakage and valve plate leakage are neglected.
4. Leakage flow path is a uniform annulus (zero eccentricity).
5. The pump operates at a constant rpm and a constant swash plate angle.
6. The hydraulic circuit operates at a constant load condition.

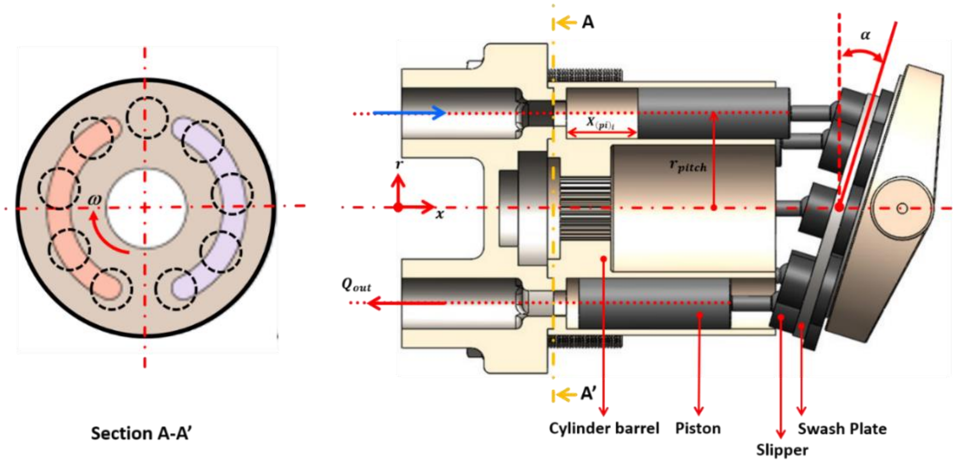

Fig. 3.1: Schematic of the axial piston pump: cross-sectional view through the center plane (right), sectional view along the plane A-A' (left).

3.3. The mathematical annular leakage flow model

The leakage path is modelled as a uniform annulus (*i.e.*, zero eccentricity) between the sliding piston and the cylinder and the entire cylinder length, as shown in Fig. 3.2. The Reynolds number for the leakage flow varies from 0.01 to 100 for the range of wear evaluated in this work. This indicates that the leakage flow is laminar. The resulting leakage model is integrated with the system network model that will help simulate the leakage from a single cylinder and a combination of cylinders thereof. The leakage flow path and the degree of fault severity in single and multiple cylinders are shown schematically in Figures 3.2 and 3.3 respectively for a few representative cases.

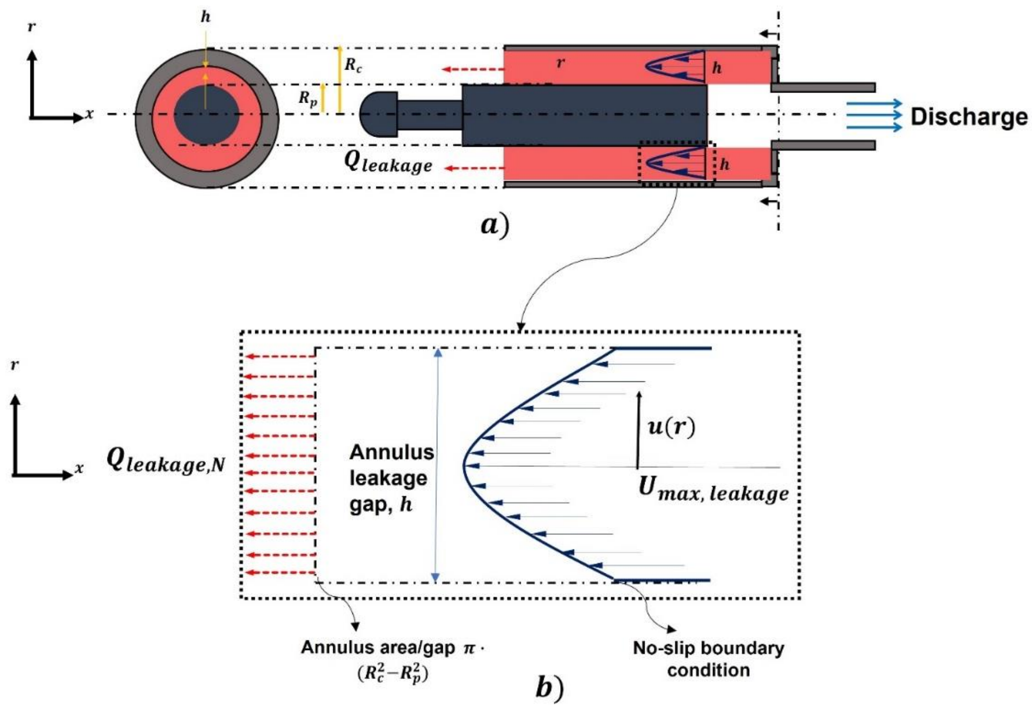

Fig. 3.2: a) Sectional view of the piston-cylinder arrangement showing the oil leakage path through a uniform annulus of width h. b) In-depth annular leakage flow path and velocity profile

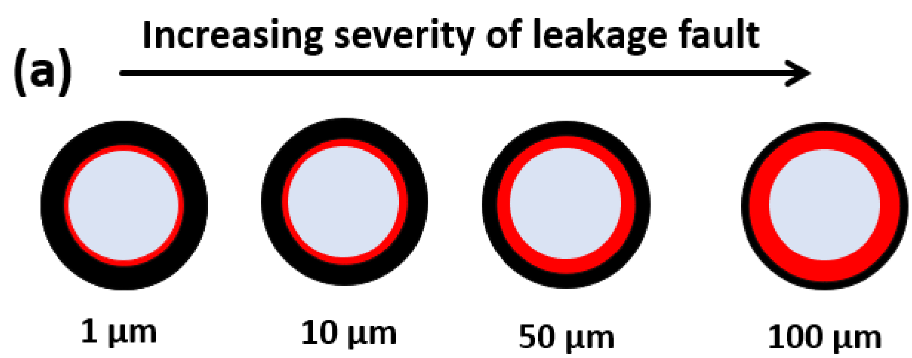

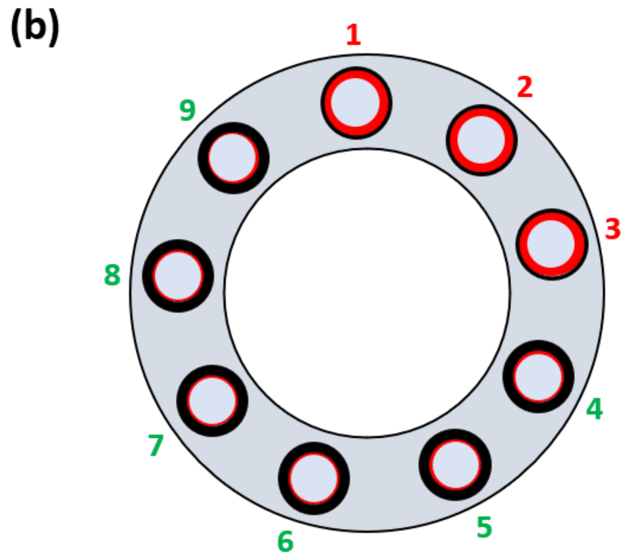

Fig. 3.3: Schematic representation of a few selective leakage fault cases investigated in this study: (a) cross-sectional view of the piston-cylinder arrangement showing increasing severity of leakage fault in a single cylinder, and (b) the complete cylinder block with leakage fault in multiple cylinders simultaneously; three faulty cylinders (1, 2 and 3: in red colour), and six healthy cylinders (4 – 9: in green colour)

Using the continuity equation and the Navier-Stokes equations for incompressible fluid flow, the formula for leakage flow rate through the annulus can be derived from the first principles [22]. Neglecting gravity and assuming axial symmetry ($^{\partial}/_{\partial\theta} = 0$), the continuity equation in cylindrical coordinates for the fully developed (radial and angular components of velocity are zero) laminar flow through the annulus is given by [23]:

$$\frac{\partial u}{\partial x} = 0 \ \text{ or } u = u(r) \text{ only} \tag{3.1}$$

With the continuity Eq. (3.1), the radial momentum equation reduces to $^{\partial P}/_{\partial r} = 0$, i.e., $P = P(x)$ only, while the x-momentum equation in cylindrical coordinates simplifies to:

$$\frac{\mu}{r}\frac{d}{dr}\left(r\frac{du}{dr}\right) = \frac{dP}{dx} \tag{3.2}$$

where, $\frac{dP}{dx} = K$ (constant) < 0. Note that in Eq. (3.1) the convective acceleration term $\rho u \frac{\partial u}{\partial x}$ is neglected because the continuity equation $\frac{\partial u}{\partial x} = 0$.

The linear Eq. (3.2) can be integrated twice to obtain the axial velocity as follows:

$$u(r) = \frac{Kr^2}{4\mu} + K_1 ln\,(r) + K_2 \tag{3.3}$$

where constants and can be obtained using the following no-slip boundary conditions at $r = R_c$ and $r = R_p$ respectively

$$u(r = R_c) = 0 = \frac{KR_c^2}{4\mu} + K_1 \ln(R_c) + K_2 \tag{3.4}$$

$$u(r = R_p) = 0 = \frac{KR_p^2}{4\mu} + K_1 \ln(R_p) + K_2 \tag{3.5}$$

The final velocity profile for leakage flow is given by:

$$u(r) = \frac{-K}{4\mu}\left[R_c^2 - r^2 + \frac{R_c^2 - R_p^2}{\ln(R_p/r)}\ln\left(\frac{R_c}{r}\right)\right] \tag{3.6}$$

Using Eq. (3.6), the leakage flow can then be calculated as:

$$= \int_{R_p}^{R_c} u(r) \cdot 2\pi r dr = \frac{-K\pi}{8\mu}\left[R_c^4 - R_p^4 - \frac{\left(R_c^2 - R_p^2\right)^2}{\ln(R_c/R_p)}\right] \tag{3.7}$$

The Eq. (3.7) can be recast in terms of the magnitude of wear (or the width of the annulus) $h = R_c - R_p$ as:

$$Q_{leakage,N} = \frac{-K\pi}{8\mu} hR_p^3(2 + \frac{h}{R_p})\left[1 + \left(1 + \frac{h}{R_p}\right)^2 - \frac{hR_p\left(2 + \frac{h}{R_p}\right)}{\ln\left(1 + \frac{h}{R_p}\right)}\right] \tag{3.8}$$

Eq. (3.8) shows that the leakage flow rate has a complex dependence on annular clearance h rather, while several previous studies [2, 6, 10] have shown that the leakage flow rate varies directly as $Q_{leakage,\ N} \propto h^3$. This difference exists because previous studies modelled the flow through the radial clearance that mimics the flow through a long, wide parallel plate in the cartesian coordinates (between piston and cylinder). However, the present approach models the leakage flow via an annular flow path in cylindrical coordinates, which better represents the leakage flow path, *i.e.*, an annulus, and therefore, presents a more realistic leakage scenario.

3.4. Mathematical model for Pump's discharge pressure/ flow

In the axial piston pump, nine pistons are nested in a circular array inside the barrel and separated by a phase angle of 40 degrees. Each piston exhibits a compound motion: linear motion inside its cylinder and rotation around the barrel axis at a constant angular speed ω. Further, in the model the APP operates at a constant load with a fixed swashplate angle of 19°. Piston's displacement and initial position depend on its angular position, *i.e.*, its phase delay at initial condition, time $t = 0$ s. Due to the tilted swashplate at a specific constant angle, each piston is located at a different position along the driveline axis at time $t = 0$ s. This initial position is given by:

$$X_{(pi)_i} = S_p - x_a \cdot \frac{r_{pitch}}{r_a} \cdot \cos(\gamma_i) \tag{3.9}$$

All pistons are arranged circularly about a common axis of rotation, called the driveline axis. The model assumes that piston 1 of the APP is located precisely at the TDC (top dead center) at the initial condition and acts as a reference point for all nine pistons. The pistons complete a pumping cycle comprising the suction half-cycle (from TDC to BDC) and the discharge half-cycle (from BDC to TDC). Since the suction (plate 1) and discharge (plate 2) valve plates are modelled separately, the phase delay angle for the piston-1 with respect to the suction side plate is set to zero, while it is 180° w.r.t to the discharge side plate. Other pistons are similarly arranged w.r.t the suction and discharge plates. The phase angle and the position of each of the pistons at the initial condition ($t = 0$ s) are listed in Table 3.1.

Table 3.1: Phase angle and position of the pistons at the initial condition ($t = 0$ s)

Piston number	Phase angle w.r.t to suction valve plate 1 (γ)	Phase angle w.r.t to discharge valve plate 2	Phase angle of swash plate	Initial position of the piston (m)
1	0°	180°	0°	0.0355
2	40°	-140°	40°	0.0365
3	80°	-100°	80°	0.0392
4	120°	-60°	120°	0.0422
5	160°	-20°	160°	0.0441
6	-160°	20°	-160°	0.0441
7	-120°	60°	-120°	0.0422
8	-80°	100°	-80°	0.0392
9	-40°	140°	-40°	0.0365

To derive the net flow rate and pressure equations for the axial piston pump the coordinate system and the geometric parameters are considered as shown in Fig. 3.1. [7] The piston's stroke (X_{pi}), velocity (V_{pi}) and acceleration (a_{pi}) which depends on the angular position (θ) as well as on the swashplate angle (α) of the APP can be expressed as follows in Eq. (3.10), Eq. (3.11) and Eq. (3.12):

$$S_p = R_p \ \cdot tan\alpha(1 - cos\theta) \tag{3.10}$$

$$\dot{S}_{pi} = V_p = \frac{dSp}{dt} = \frac{dS_P}{d\theta} \times \frac{d\theta}{dt} = \frac{dSp}{dt} \cdot \omega_p \tag{3.11}$$

$$\ddot{S}_{pi} = a_p = \frac{d\dot{S}p}{dtt} = \frac{d\dot{S}_P}{d\theta} \cdot \frac{d\theta}{\alpha t} = \frac{d\dot{S}p}{d\theta} \cdot \dot{\omega}_p \tag{3.12}$$

The kinematical flow rate from the single piston along the direction of the piston axis can be expressed as:

$$Q_{kp} = A \cdot V_p = \dot{S}p \cdot \frac{\pi}{4} D_p^2 \tag{3.13}$$

$$Q_{kp} = \omega \cdot \frac{\pi}{4} D_p^2 \cdot r_{pitch} \cdot tan\alpha \cdot sin(\omega t) \tag{3.14}$$

$$\theta = \omega t \tag{3.15}$$

The flow rate from an individual piston is delayed by the phase angle (δ), and the flow rate from the i^{th} number of pistons is given by Eq. (3.16):

$$Q_{kp,i} = \omega \cdot \frac{\pi}{4} \cdot D_p^2 \cdot r_{pitch} \cdot tan\alpha \cdot si\,n(\omega t - (i-1) \cdot \delta) \tag{3.16}$$

The total or the net kinematical flow discharge, which is the combined discharge (kinematic) from all nine pistons individually is given by [7]:

$$Q_{net,k} = \omega\pi \cdot R_p^2 \cdot r_{pitch} \tan\alpha \sum_{i=0}^{n-1} \sin(\omega t - i\delta) \tag{3.17}$$

Note that for a fixed swash plate angle and a given pitch radius of the cylinders, the length of the pistons must be greater than the stroke length, and therefore, in the model the piston length is considered greater than the stroke length corresponding to a fixed swash plate angle of 19°.

The phase angle (δ) between each cylinder (equally distributed), the pressure inside the piston chamber, the flow rate from the piston chamber to the discharge chamber of each piston, and the total flow rate to the discharge chamber are Eq. (3.18), Eq. (3.19) and Eq. (3.20) respectively. And where, A_d represents the orifice area of each cylinder as varies depending on the angular position of the cylinder, as detailed in Ref. [7]. Based on the continuity equation in the cylinder chamber, the instantaneous pressure (P_{pi}) inside i^{th} cylinder can be expressed as:

$$\delta = \frac{2\pi}{i} = \frac{360°}{9} = 40° \tag{3.18}$$

$$\dot{P}_{pc,i} = \frac{K_b}{V_0 - A_{p_i} \cdot X_{p_i}} \cdot \left(Q_{kp} - Q_{pc} - Q_{leakage}\right)_i \tag{3.19}$$

$$(Q_{pc})_i = C_d \cdot A_{d_i} \cdot \sqrt{\frac{2|P_{pc,i}-P_{out}|}{\rho}} \cdot \text{sgn}\,(P_{pc,i} - P_{out}) \tag{3.20}$$

$$Q_{pc_{net}} = \sum_{N=1}^{N=9} (Q_{pc})_i \tag{3.21}$$

3.5. Model for the load condition

The flow rate and the pump's outlet pressure, which are the key flow parameters for leakage fault diagnosis of an axial piston pump, can be determined by substituting the fluid properties, the geometrical, and the operating parameters of the pump with the following equations (3.22).

$$\dot{P}_{out} = \frac{K_b}{V_{Ch}} (Q_{pc_{net}} - Q_{out}) \tag{3.22}$$

$$Q_{out} = C_d \cdot A_{load} \cdot \sqrt{\frac{2 \cdot P_{out}}{\rho_{fluid}}} \tag{3.23}$$

The initial clearance volume of the cylinder at the top dead center is given by:

$$V_{c,i} = V_{dead} + A_p \cdot 2R_{p,i} \cdot \tan\alpha \tag{3.24}$$

3.6. Summary

This chapter has demonstrated how to develop the total mathematical model equations for an axial piston pump's total kinematic, leakage flow, and load conditions. Then, in the next chapter, the actual simulation working model of an axial piston pump is detailed, based on all the driven equations and utilized parameters in this chapter 3.

Chapter 4

Simulation: Leakage conditions in APP

4.1. Introduction

This chapter describes a simulation approach for a nine-piston axial pump in the MATLAB-Simscape environment, based on the mathematical equations developed in previous chapter 3. This simulation model is designed to simulate the effect of increasing the severity of a leakage fault (growing the annular gap) on pump performance in both single and multiple cylinders simultaneously under various possible faulty piston configurations.

4.2. Simulation-modelling approach and methodology

A closed-loop flow network architecture of the APP's hydraulic control system involving a variable displacement axial piston pump is developed using Simscape; in the Simulink environment of MATLAB 2020b. Leakage via the clearance between the piston and cylinder is modelled as laminar flow through a uniform annulus, accounting for varying severity of leakage fault from 1 μm to 100 μm. The simulation results from this model are presented in terms of the trends in the time-mean value of the pressure and the flow rate at the pump outlet and the changes in their time-varying waveforms as a function of the severity of leakage fault in single and multiple cylinders.

The system network model comprises a closed-loop hydraulic circuit, the axial piston pump, and a single piston-cylinder assembly with a block representation of the physical components. The hydraulic model is integrated with an overall system network model to simulate the severity of leakage fault in single and multiple cylinders and evaluate the pump performance in response to the fault. The lower part of Fig. 4.1 represents the signal display-cum-logging panels for pressure and flow signals. The flow and pressure signals for each of the 9-pistons and the net discharge flow and pressure signals resulting from a given leakage condition simulation are displayed and logged on the flow and pressure panels, respectively. The hydraulic model is further composed of the leakage flow model, the pump discharge and pressure model, and the model for the load condition.

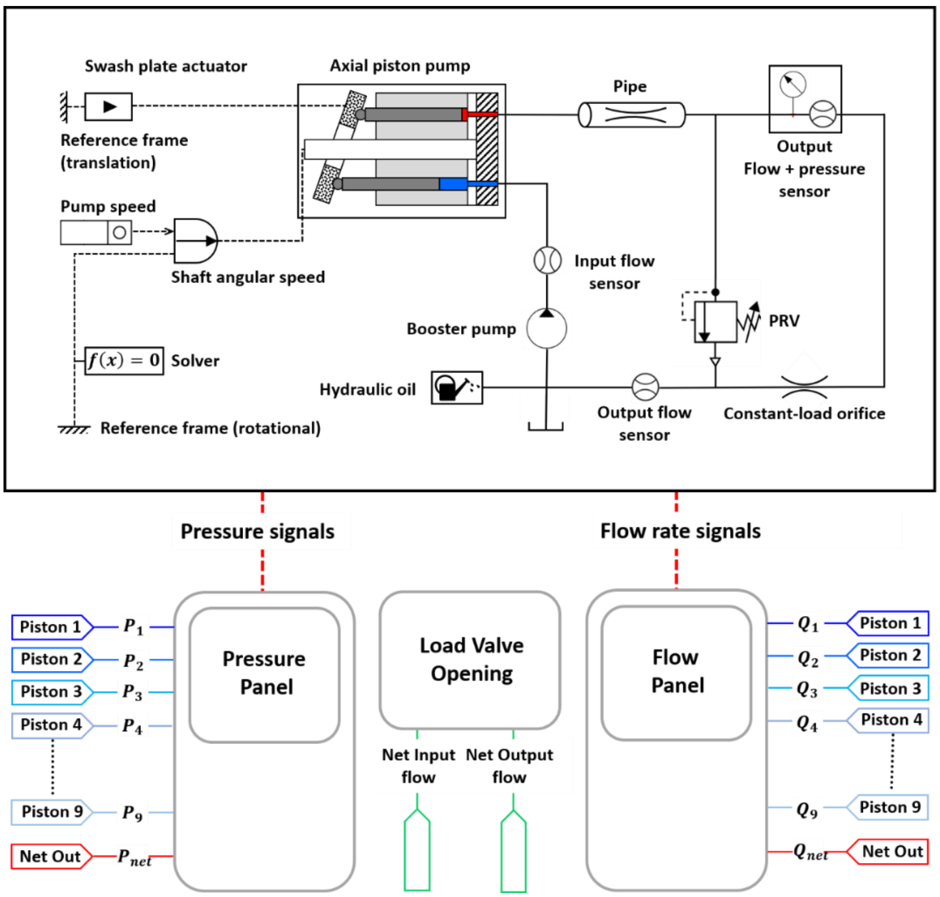

Fig. 4.1: Block model of the hydraulic system network for simulation of leakage fault in an axial piston pump with different degree of wear in single and multiple cylinders.

4.3. Parameters used for simulating/mimic axial piston pump

The simulations are performed in the MATLAB R2020b-based modelling environment Simulink 10.2 using the backward-Euler implicit method with a fixed time step of 10-4 s. For each test case, the simulation time is 0.1 s, which corresponds to ~ 4 pumping cycles (0.024 s per cycle) for a rotational speed of 2500 rpm. However, for brevity, the simulated waveforms of outlet pressure and flow are presented for at most 3 pumping cycles (~ 0.1 s) for all test cases. The different parameters and operating conditions used as inputs to the model are detailed in Table 4.1. Note that while the majority of these initialization parameters are selected directly based on the specifications of industrial axial piston pumps [25 - 27], a few others are determined to satisfy the geometric constraints

Table 4.1: System parameters used for simulating leakage fault in an axial piston pump.

	Parameter	Symbol	Magnitude (unit)
Fluid and Flow properties	Temperature of fluid	T	60 ℃
	The density of the hydraulic fluid	ρ_{fluid}	960 kg/m^3
	Isothermal bulk modulus	K_b	1.25 Gpa
	Kinematic viscosity	v	7.2 cSt
	Volume fraction of entrained air	-	0.20 %
	Density of air	ρ_{air}	1.225 kg/m^3
	Critical Reynolds number	Re_{cr}	150
	Discharge coefficient	C_d	0.64
Pump specifications	Number of cylinders/pistons	i	9
	Cylinder pitch radius	r_{pitch}	0.022 m
	Cylinder orifice diameter	D_d	0.01032 m
	Intial Piston diameter $_{\text{max leakage gap}}$	D_p	$0.01031\,{}^{\;\;0}_{-0.0002}$ m
	Piston stroke	S_p	0.08 m

	Piston length (excluding piston rod)	-	0.014 m
	Piston dead volume	V_{dead}	0.0002504 m^3
	Phase delay	δ	40°
	Swashplate angle	α	19°
Operating conditions	Rotational speed	ω	2500 rpm
	Constant load	-	Yes
	Booster pump discharge pressure	-	0.5 Mpa
	Drain tank pressure	-	0.1 Mpa

4.4. APPs control System network model

4.4.1. Model for the closed-loop hydraulic circuit

The leakage fault simulation is based on a simple closed-loop flow network as shown in Fig. 4.1. It consists of an axial piston pump that draws fluid from the booster pump and delivers it to the drain tank via a constant load orifice. The suction port (low-pressure side) of the pump is attached to the discharge of a booster pump, which ensures that the necessary pressure is maintained at the suction of APP at the test speed (2500 rpm). The booster pump operates at a constant pressure differential of 0.5 MPa, withdrawing fluid from the drain tank at 0.1 MPa and delivering the fluid directly to the APP suction at 0.5 MPa. The pump's discharge port (high-pressure side) delivers the fluid back to the drain tank (set at atmospheric pressure: 0.1 MPa) via the constant load orifice that controls the hydraulic circuit's constant load condition. The constant load is set by fixing the orifice area. During the suction stroke (from TDC to the BDC), the cylinder pressure is very low, and therefore, the pressure difference between the cylinder and the drain is insufficient to cause any significant leakage.

In contrast, during the discharge stroke (from BDC to TDC), the cylinder pressure is much higher than the drain, causing leakage. This way, with respect to a single cylinder, the leakage occurs only during one-half (discharge) of the pumping cycle. This complete loop allows the pump to simulate the leakage faults and analyses the discharge flow and pressure ripples.

4.4.2. Model for the axial piston pump

The model of the axial piston pump consists of nine piston-cylinder subsystems ($i = 1, 2, 3 \ldots .9$) that are modelled individually, as shown in Fig. 4.2. Each subsystem model is connected to four different external ports: pump suction port (a low-pressure side: Port S), Pump discharge port (high-pressure side: Port D), fixed swash plate source (Port B), and the pump driving shaft (Port A). The suction port (Port S) of all the cylinders is connected to the delivery side of the booster pump. The discharge port (Port D) of all the cylinders is connected to a flow-pressure sensor that measures the flow rate and pressure at the pump discharge.

Since a key objective of the study is to capture the sole effect of the severity of leakage fault on the dynamic response signals (flow and pressure) at the pump outlet, the displacement control mechanisms such as the pressure compensator or servo valve or the load sensing mechanisms are not incorporated in the model of the APP. Otherwise, these mechanisms will change the swash plate angle in response to the changes in the dynamic response signals caused by the leakage fault. Consequently, the signals will be modulated (due to the swashplate movement), which will not represent the sole effect of leakage fault. Therefore, the APP is modelled as a fixed displacement pump with a fixed swashplate angle of 19°. For the same reason, the pump response to leakage fault is investigated under a constant load condition.

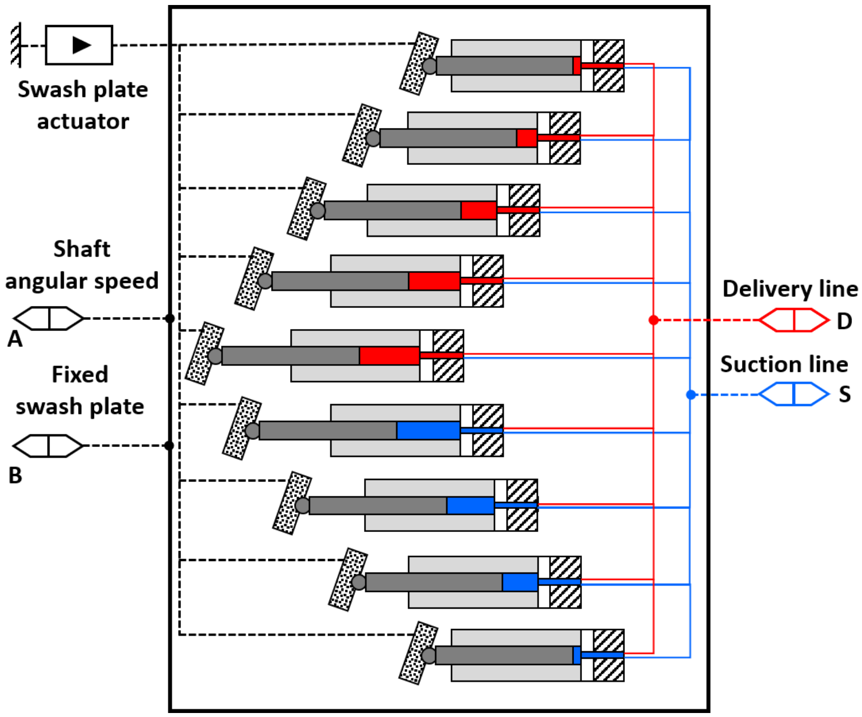

Fig. 4.2: Simscape block model of an axial piston pump with nine pistons

4.4.3. Model of a single piston-cylinder assembly

The model of a single piston-cylinder assembly developed in Simscape is illustrated in Fig. 4.3. The model consists of a single-acting hydraulic cylinder connected separately to the valve plates 1 and 2 at the suction and the discharge side, respectively. The valves plate geometry is modelled with kidney-shaped suction and discharge ports that run between the pressure carry-over angle and 180°. The two-valve plates are separated by a phase angle of 180° and allow the suction and discharge to be modelled separately. The pump delivery line has flow and pressure sensors for transmitting the time-varying flow rate and pressure waveforms at the pump outlet. The other side of the piston-cylinder block is connected mechanically to a swashplate block and an angular motion sensor. This same model is repeated for all 9 pistons, each separated by a phase angle of 40° and distributed evenly along the periphery of the cylinder block.

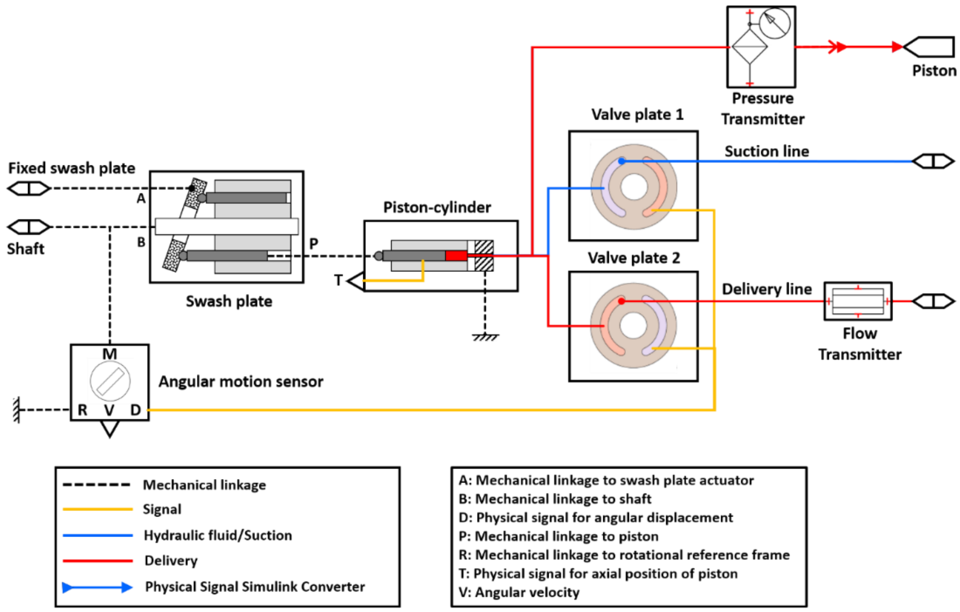

Fig. 4.3: Simscape block model of a single piston-cylinder assembly with the interfacing mechanical linkages, hydraulic lines, signal lines and flow and pressure sensors.

4.5. Model Validation

4.5.1. Parameters for model validation

In section 3.4, the model's suitability for leakage fault detection is assessed by comparing the model-predicted waveforms of the pressure at the output of each cylinder and the net pressure output at the pump discharge with the experimental results of Bergada et al. [10]. Their experimental set-up consisted of a Vickers PVB5 axial piston pump with 9 cylinders. The experimental parameters reported in Ref. [10] are listed below in Table 4.2, used as model inputs.

Table 4.2: Parameters reported in Ref. [10] and used as model inputs for validation.

	Parameter	Magnitude (unit)
Fluid and Flow properties	Fluid type	Hydraulic oil ISO 32
	Temperature of fluid	37 °C
	The density of the hydraulic fluid	857 kg/m^3
	Isothermal bulk modulus	1.8 x 10^9 Mpa
	Kinematic viscosity	32 cSt
	Volume fraction of entrained air	0.2 %
	Density of air	1.225 kg/m^3
	Discharge coefficient	0.6
Pump specifications	Number of pistons	9
	Cylinder pitch radius	0.0221 m
	Cylinder orifice radius	0.0051 m
	Initial piston diameter	0.0103 m
	Piston stroke	0.08 m
	Piston length (excluding piston rod)	0.014 m
	Piston dead volume	2.504 x 10^{-7} m^3
	Phase delay	40°
	Swashplate angle	20°
Operating conditions	Rotational speed	1000 rpm
	Constant load	Yes
	Drain tank pressure	0.1 Mpa

4.5.2. Comparison between model and experimental studies

Their experimental set-up consisted of a nine piston Vickers PVB5 pump operating at 1000 rpm at a fixed swash plate angle of 20° and using hydraulic mineral oil ISO 32 was tested. The pump operated under constant load conditions of 2, 5, and 10 MPa, which was achieved by fixing the discharge orifice area of the needle valve in the hydraulic circuit. The transient pressure in each cylinder was measured by installing an absolute pressure transducer at the discharge end of the cylinder with its sensing port aligned along the cylinder axis. To measure the pressure and flow rate at the pump discharge, a pressure transducer, and a high-response Kracht flow meter were mounted in the pump discharge line immediately upstream and downstream of the pressure relief valve. The dynamic pressure signals in a single cylinder and at the pump outlet were measured for an annular clearance of 5 μm. To mimic a leakage fault scenario due to a worn piston, four levels of wear, *i.e.*, a uniform annular gap of 5 μm, 6 μm, 7 μm, and 10 μm for a single piston was numerically simulated. The changes in the output flow ripples in response to these different levels of wear were presented. To compare the model predictions of dynamic pressure waveforms with the experimental results presented in Ref. [10], a representative case of $h = 5\ \mu m$ is chosen. The parameters reported in Ref. [10] used as inputs to the model are listed in Table 4.2.

The comparison of model predictions and the experimental results is presented in Fig. 4.4 and 4.5, in which the time-varying signature of the pressure in a single cylinder and the net pressure at the pump outlet for a fault severity of $h = 5\ \mu m$ in a single-cylinder, respectively.

In both cases, the model accurately captures all the critical features of the experiments. For a single cylinder, the model simulated cycle time and the amplitude of the pressure signal show an excellent match with the experimental signal. The model accurately predicts the cycle time to be 0.06 s.

However, the maximum relative error in the magnitude of pressure is ~10.6 % across the entire signal. Like the single cylinder case, the model prediction of the net pressure signal follows the same trend as the experimental signal as both have the same period. In addition, the relative error in the pressure magnitude is not more than ~9.5 % at any time instant between the model and the experimental result. Based on these comparisons we conclude that the results from the model can capture the behavioral trends observed in experiments, and therefore, the model can be utilized to understand the effect of leakage fault severity in single and multiple cylinders on the pump performance.

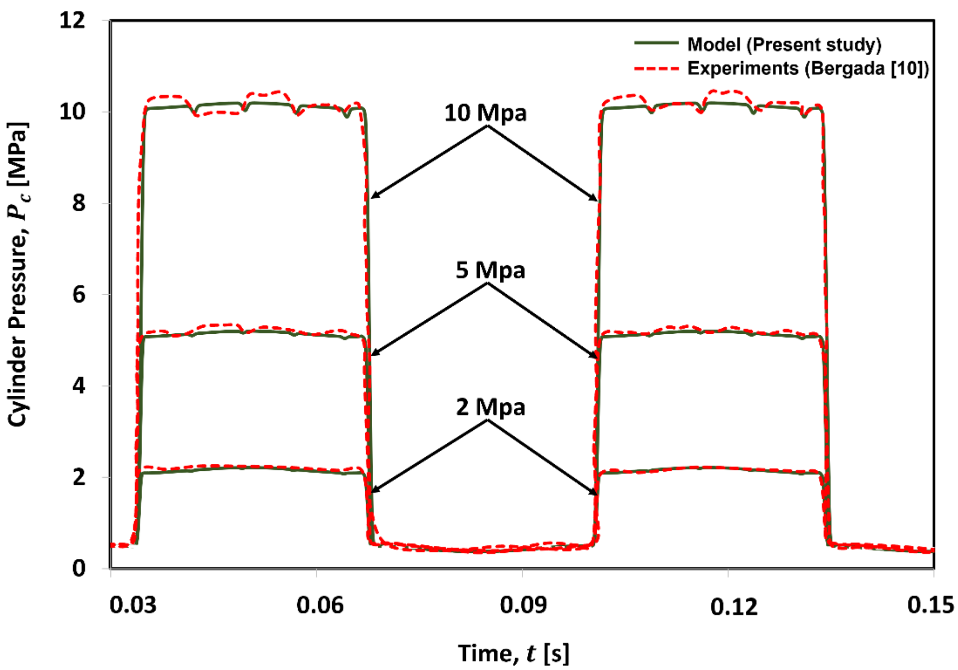

Fig. 4.4: Dynamic pressure signal (at APP output conditions **2, 5, and 10** Mpa) comparison between the current study's model predictions (solid line) and the experimental data (dotted line) of Ref. [10] for a single-cylinder (top) and at the pump outlet (bottom).

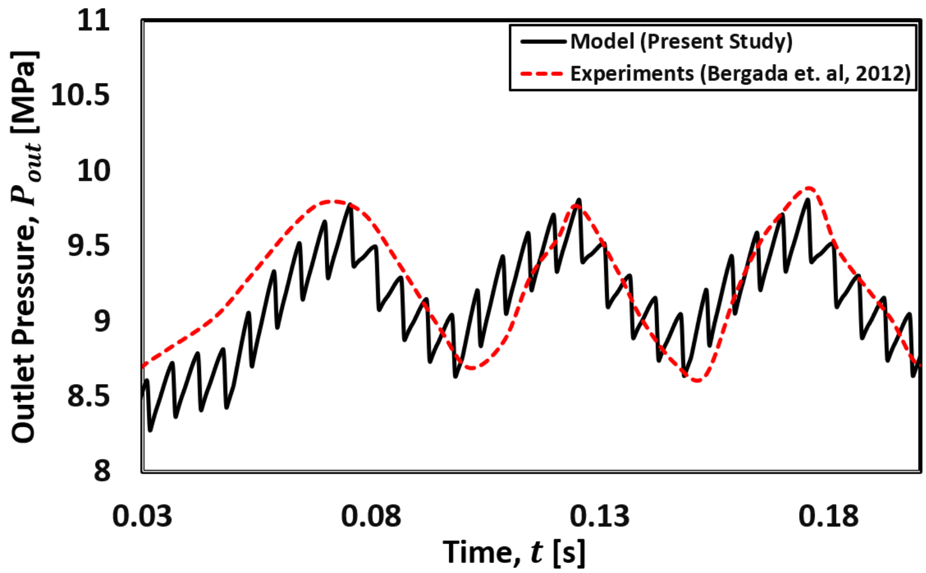

Fig. 4.5: Comparison of dynamic pressure signal between the model predictions (solid line) of the current study and the experimental results (dotted line) of Ref. [10] for a single-cylinder (top) and at the pump outlet (bottom).

4.6. Summary

This chapter demonstrates how to build a working simulation model of an axial piston pump in the MATLAB-Simscape environment by applying all the driven equations and actual parameters to simulate this model with real-world working circumstances. Furthermore, the comparison of model predictions and experimental findings is provided in this chapter, which includes the time-varying signature of the pressure in a single cylinder and the net pressure at the pump output. Moreover, the severity of leakage faults in single and multiple cylinders is then explored in the subsequent chapter.

Chapter 5

Leakage fault severity: In single and multiple cylinders

5.1. Introduction

Axial piston pumps are at the core of power hydraulics due to their ability to generate high pressures and accommodate control circuits intrinsically, which can alter the swash plate angle dynamically to regulate the flow and pressure and help in controlling the speed of hydraulic motors and actuators. However, to accomplish these high-precision tasks, they are designed with extremely tight tolerances between the parts (in relative motion), making them susceptible to wear and hence, leakage. Existing efforts for diagnosing leakage faults and predicting pump performance have been typically restricted to studies that assume arbitrary values of the severity of leakage. In few approaches that have considered the effect of leakage fault severity still do not incorporate the effects of leakage fault in multiple cylinders (as shown in Fig. 5.1) simultaneously. Despite the recent investigations that have pointed toward the importance of leakage fault diagnosis in piston pumps, none have explored the collective role of two fault parameters on the pump performance, namely, the growing severity of leakage fault and the number of faulty cylinders.

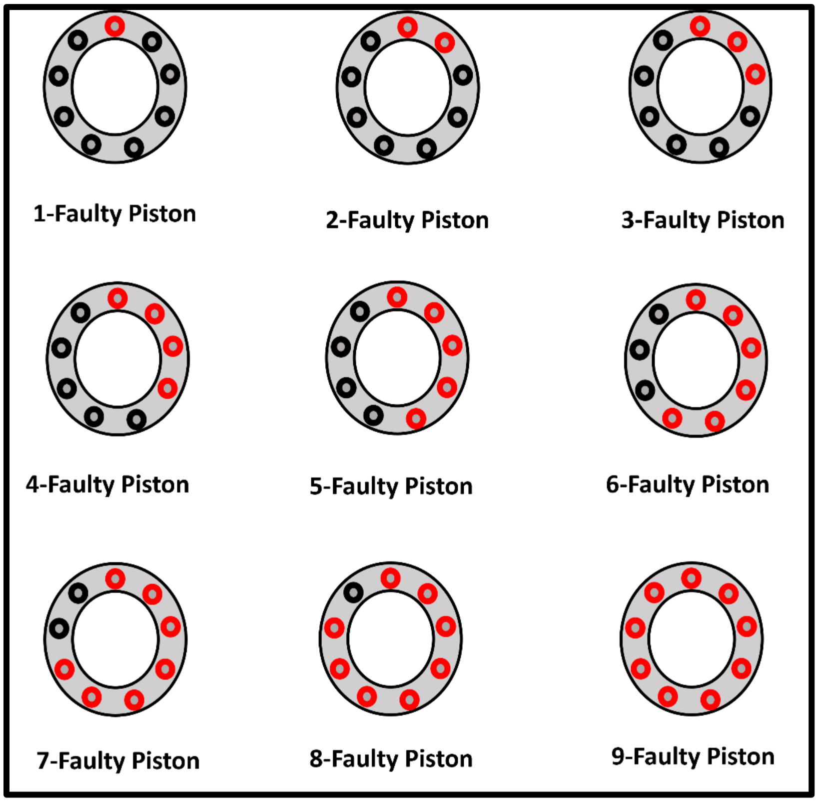

Fig. 5.1: Schematics for cylinder's cross-sectional view with N = (1 to 9) numbers of faulty piston-cylinder in an axial piston pump.

5.2. Results and Discussion

5.2.1. Dynamic signals response analysis

In this section, the representative plots that help visualize and understand the effect of increasing severity of leakage fault are shown in Fig. 5.2 separately for single (left) and multiple pistons (right). The top row shows the dynamic flow rate signals, while the bottom row shows the plots for dynamic pressure signals. In each plot, the signals (flow rate or pressure) for the individual cylinders as well as the net output signal are shown simultaneously, where the continuous lines represent the healthy condition while the dotted lines represent the faulty condition. For instance, in Fig. 5.2 (a1), the waveforms at the bottom represent the rectified sinewaves of the flow rate delivered by each of the nine pistons individually, each separated by

0.0026 s (corresponding to a phase delay of 40 degrees). In the same Fig. 5.2 (a1), the waveform on the top (solid green curve) represents the net flow at the pump outlet due to the cumulative effect of all nine pistons. It is apparent from this plot that over a time duration of one pumping cycle (~ 0.024s), nine ripples are observed in the signal. The flow rate waveform of a single faulty cylinder (cylinder #1 with fault severity or annular clearance of $h = 60$ µm) represented by a dotted curve indicates that there is a drop in the flow rate of cylinder #1, which causes a corresponding reduction in the net flow rate (see red dotted curve). Fig. 5.2 (b1) shows that with the same level of fault severity ($h = 60$ µm) in two cylinders, the net flow rate reduces significantly (red dotted line). Similarly, the bottom two plots for pressure at the pump outlet demonstrate a similar trend; see Figures 5.2 (b1) and (b2). With this basic understanding of the representative plots, the effect of the severity of leakage fault on the time-varying behavior of the pump is discussed next.

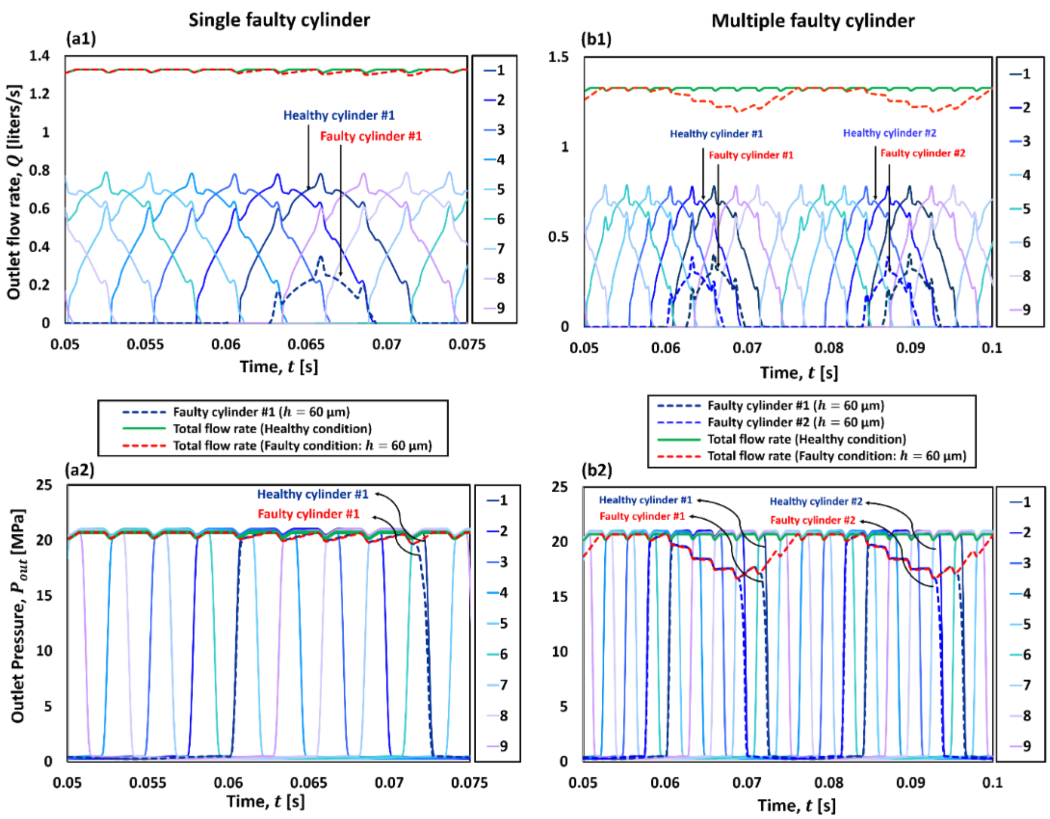

Fig. 5.2: Dynamic response signals of individual cylinders and their net output at the pump discharge for a single faulty cylinder (left) and multiple faulty cylinders (right: representative for two faulty cylinders). The leakage fault severity for both cases is $h = 60$ μm. The top and bottom rows represent the temporal variation of flow rate and pressure, respectively.

The changes in the dynamic behavior in response to the variation in the degree of leakage are characterized by changes in the amplitude and frequency of the outlet flow rate and pressure waveforms. To simulate different degrees of an oil leakage fault, the annular clearance (h) is varied over two orders of magnitude 1 μm – 100 μm: in increments of ~10 $microns$. Here, h = 1 μm corresponds to a healthy pump condition and forms the baseline case against which the other cases will be compared.

5.2.1.1. Leakage fault signals in a single cylinder

Fig. 5.3 shows the variation in the dynamic waveforms of pressure at the pump outlet with the increasing degree of oil leakage fault in a single cylinder. Recall from Fig. 5.2 that in comparing the healthy versus leakage fault conditions, it is apparent that the oil leakage fault causes a reduction in both the outlet flow and pressure. However, this reduction is more pronounced in the case of the pressure signal. Furthermore, pressure sensors are seldom installed for individual cylinders to acquire the corresponding instantaneous signals in practice. This is because such an arrangement would require additional high-pressure sensing lines per cylinder to be routed through a compact pump, significantly increasing the design complexity. Instead, the pressure signals at the pump outlet are easy to acquire and can be monitored and analyzed to determine the pump's health [6, 7]. With the h = 1 μm as the healthy baseline condition and focusing on one pumping cycle, say from 0.082 s to 0.1 s (see the zoomed view at the top in Fig. 4.2), the following features are apparent from Fig. 5.5: First, the output pressure signal decreases non-linearly with increasing severity of leakage fault. Starting with h = 1 μm, as the severity of leakage fault increases, no decrease in pressure is observed up to $h \cong 40$ μm, which is seen by the output pressure signals for $h = 10$ μm, 20 μm, 30 μm lying exactly on top of the baseline healthy signal. At h = 40 μm, a reduction (although small) is first observed in the pressure signal compared to the healthy baseline signal for h = 1 μm. With a further increase in the severity of the leakage fault, *i.e.*, beyond h = 40 μm, the pressure signal drops significantly below the baseline signal over a range of 40 μm $< h <$ 80 μm. Finally, in the extreme condition of $h \geq 80$ μm, a point is reached where the output pressure signal drops to such an extent that it can barely recover back to its original magnitude, as in the healthy condition. The pressure recovers back to its magnitude as in the healthy signal only momentarily before it begins to drop again. For example, as shown in Fig. 5.2, at $h = 100$ μm, the pressure starts to drop at the beginning of a pumping cycle (first ripple) and recovers not until the end of the cycle (last ripple), following which it starts dropping again immediately within the time span of the same ripple, *i.e.*, in less than $0.0026\ s$. In summary, the drop in the pressure signal occurs non-linearly in three stages with increasing severity of the leakage fault: Stage I ($h \leq 40$ μm), where the pressure signal is identical to the healthy signal, Stage II (40 µm $< h < 80\ \mu m$), where the pressure signal drops markedly with increasing faulty severity, and Stage III ($h \geq 80\ \mu m$), where the pressure signal drops to such an extreme level that it can barely recover. With respect to a single faulty cylinder, these stages (I, II, and III) correspond to the healthy condition, moderately faulty condition, and severe faulty condition of the axial piston pump. The existence of three stages indicates that for a piston pump with a single faulty cylinder, there exist two threshold values of the leakage fault, one at $h\ \cong 40\ \mu m$; the threshold value at which the pressure shows first signs of reduction, and a second at $h\ \cong 80\ \mu m$; the critical threshold beyond which the pressure drops to extremely low magnitudes such that it can hardly recover during a pumping cycle. Note that while the two threshold values exist for a piston pump, their absolute value would depend on the specific pump type and may differ from one pump to another.

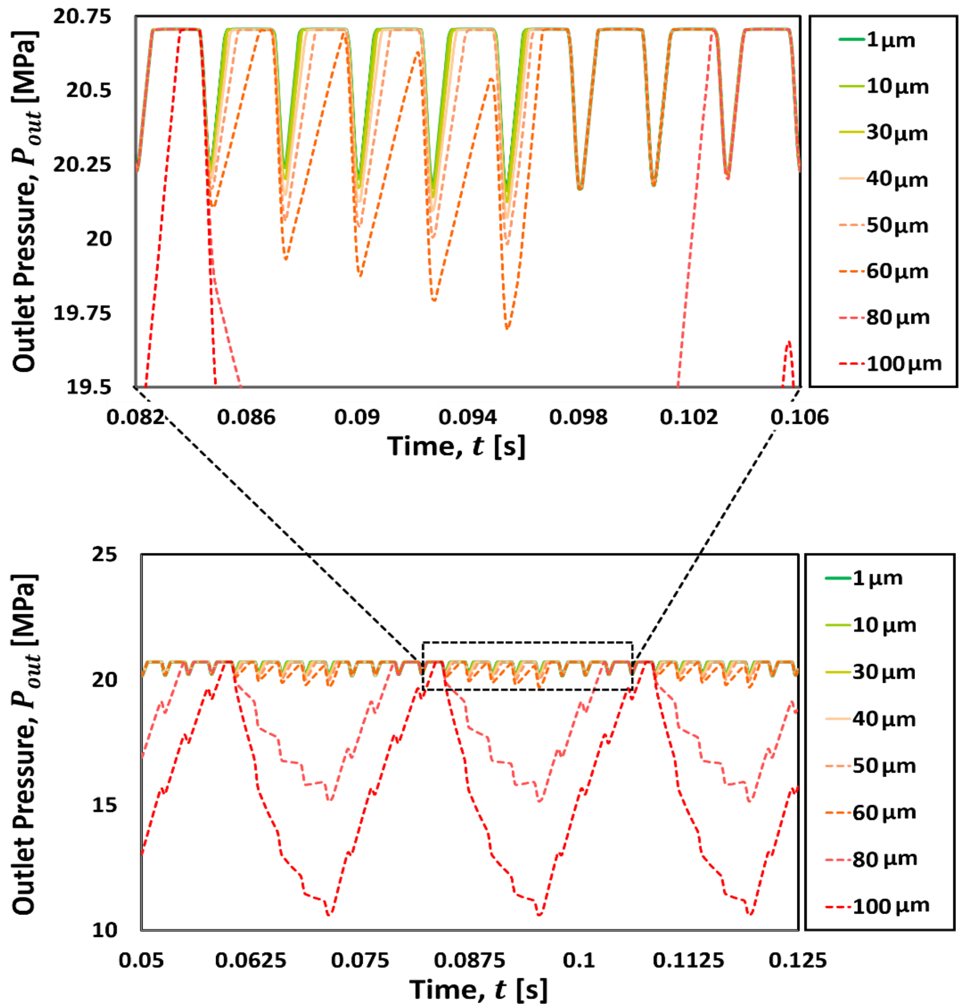

Fig. 5.3: Dynamic pressure signal at the pump outlet at different degrees of leakage fault: (Top) for one pumping cycle. (Bottom) for three pumping cycles.

The faulty condition of the pump, *i.e.*, Stage II (40 µm $< h <$ 80 µm) and Stage III ($h \geq$ 80 µm), are particularly interesting because they indicate that increasing the fault severity not only reduces the output pressure (which is expected) but it also alters the time signature of the pressure waveform. This can be explained as follows: From a pressure signal point-of-view, a pumping cycle comprises pressure-decay, pressure-build-up, and pressure restoration, that occur sequentially. This is shown in Fig. 5.4 for two representative values of fault severity: $h =$ 60 µm and 80 µm. Physically, the pressure-decay corresponds to the duration between the faulty piston entering and leaving the pump's discharge port. Next, the pressure-build-up duration is the one in which the faulty piston moves to the suction port while the healthy pistons in the discharge port try to recover the decreased pressure back to its initial magnitude. The remaining time in the pumping cycle is the pressure-restoration period, where the output pressure has recovered and remains at its initial value as in the baseline healthy condition. Fig. 5.4 shows that the larger the severity of leakage fault, the larger the drop in the pressure magnitude, and therefore, more will be the number of healthy pistons (and hence the time) required to restore the pressure. This means that the pressure-build-up time increases with fault severity, or alternatively, the pressure-restoration time reduces.

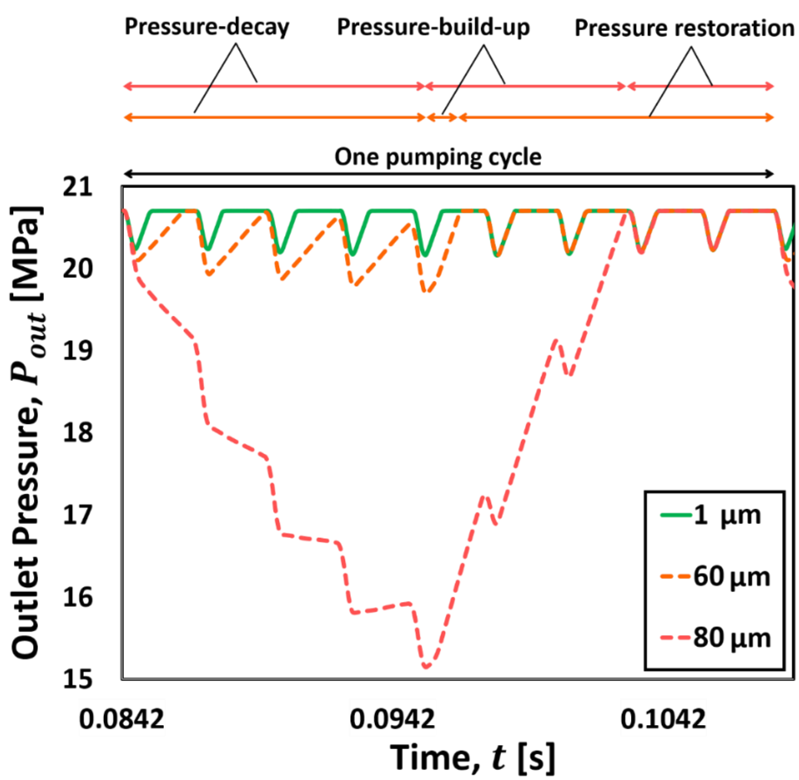

Fig. 5.4: Temporal variation of the net pressure at the pump outlet over one pumping cycle. The pressure-decay, pressure-build-up, and pressure restoration for two faulty conditions (h = 60 µm and 80 µm) are shown marked.

For instance, over one pumping cycle, the pressure-build-up time for $h = 40\ \mu m, 60\ \mu m\ and\ 80\ \mu m$ is $\Delta t =$ 0.0007 s, 0.0012 s, and 0.0075 s, respectively. From Fig. 5.4 and based on these pressure-build-up times, once the faulty cylinder leaves the discharge port at $t =$ 0.0955 s, with $h = 60$ µm, less than one healthy cylinder is required to restore the pressure, while with $h = 80\ \mu m$, approximately three healthy cylinders are required for restoring the pressure. Under extreme leakage fault (see for example, $h = 100$ μm), the pressure drops to such low magnitudes that even with the following four healthy pistons, the pressure manages to recover just momentarily. Furthermore, another consequence of the leakage fault is that as the pressure drops to lower and lower magnitudes with increasing fault severity, the peak-to-peak amplitude of the pressure waveform increases, and the time-mean value decreases (see figures 5.3 and 5.4). Therefore, for a given number of cylinders, pump rpm and the constant load condition, a direct consequence of the increasing severity of leakage fault in a single cylinder is that the output pressure waveform gets altered such that both its peak-to-peak amplitude and the pressure-build-up time increase, while its time-mean value decreases.

5.2.1.2. Leakage fault signals in multiple cylinders

The wear in a single cylinder is the simplest case of leakage fault in an axial piston pump and allowed a detailed explanation of the effect of increasing faulty severity on the discharge pressure waveforms. However, in practical applications, the leakage fault may occur in multiple cylinders simultaneously, each having a different fault severity level, complicating the fault diagnosis process. Therefore, this section presents a mechanistic understanding of the effect of leakage fault in multiple cylinders on the waveform of net pressure at the pump outlet as a function of the severity of leakage fault.

For brevity, Fig. 5.5 shows the time-varying pressure signals for six representative levels of fault severity ($h = 1$ µm, 30 µm, 40 µm, 50 µm, 60 µm and 80 µm). In each plot, the green-colored pressure waveform represents the healthy baseline case with no faulty cylinder, while the other curves represent pressure waveforms corresponding to the different number of faulty cylinders. In Figures 5.5 (a) and (b) for $h = 1$ µm and 30 µm, respectively, the pressure waveforms for all sets of faulty cylinders fall on top of the healthy signal. This indicates that at these low levels of fault severity, the pump behaves the same as it would in the healthy condition even with the leakage fault in all its cylinders, *i.e.,* all nine cylinders. On moving to $h = 40$ µm (see Fig. 5.5 c), a slight drop in the pressure is first observed with an increasing number of faulty cylinders. For $h = 40$ µm and higher values, the following key observation can be drawn from Fig. 5.5: First, at any given level of fault severity, the magnitude of pressure drop increases with increasing number of faulty cylinders in each pumping cycle. This is evident by a continuous downward shift in the pressure signals. A direct consequence of this increased pressure drop is that the pressure-decay plus the pressure build-up time increases with the increasing number of faulty cylinders. Second, for each fault severity level, the pressure signal's peak-to-peak amplitude increases with increasing number of faulty cylinders up to four faulty cylinders and then decreases. Third, for each level of fault severity beyond $h = 40$ µm, there exists a certain maximum number of faulty cylinders beyond which the pressure signal cannot recover back to its initial value as in the healthy state. Further, the magnitude of this maximum number of faulty cylinders decreases with increase in fault severity. Specifically, the number of faulty cylinders that pump can afford while being able to recover the pressure is nine (all faulty cylinders) for $h \leq 40$ µm, three to four for $h = 50$ µm, two for $h = 60$ µm, and just one faulty cylinder in the extreme case of $h \geq 80$ µm, where the pressure recovers for a concise moment ~ 0.0013 s.

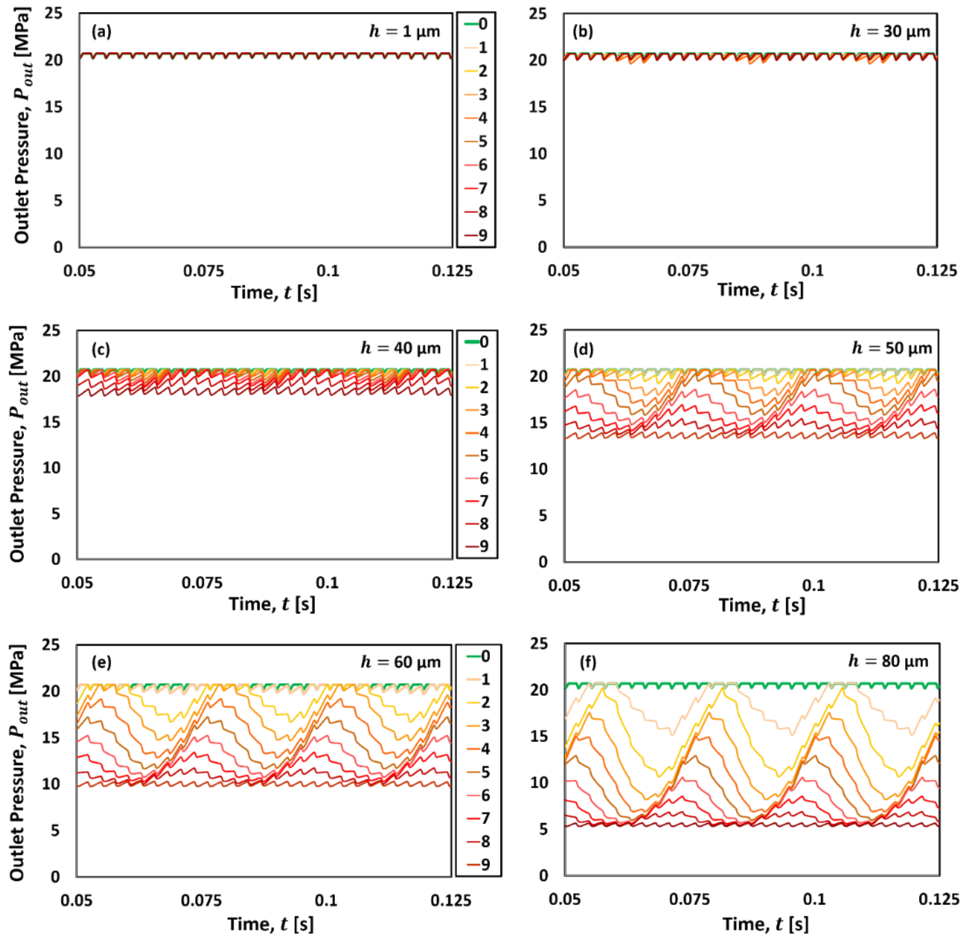

Fig. 5.5: Temporal variation of the net pressure at the pump outlet with increasing number of faulty cylinders, at different levels of fault severity: (a) $h = 1$ µm, (b) $h = 30$ µm, (c) $h = 40$ µm, (d) $h = 50$ µm, (e) $h = 60$ µm, and (f) $h = 80$ µm.

While the dynamic response signals reflect the changes in amplitude and frequency of pressure waveforms in response to the leakage fault, they do not capture the trends in pump performance as a function of the cumulative effect of fault severity and the number of faulty cylinders. This outlines the focus of the next section.

5.2.2. Time-mean response analysis

Figure 5.6 shows the variation in the time-mean flow rate and pressure at the pump discharge with both the leakage fault parameters, namely, the fault severity and the number of faulty cylinders in the pump. In comparing Figures 5.6 (a) and (b), it is apparent that the flow rate and pressure exhibit the same trends, and therefore, for brevity, only Fig. 5.6 (a) is discussed next to explain the pump's time-mean response to the fault parameters. Following trends can be identified from Fig. 5.6 (a): First, irrespective of the number of cylinders in the pump that are faulty, there exists a critical threshold magnitude of the leakage fault severity (annular clearance) below which the flow rate remains nearly constant and equals its value in the healthy condition. For the pump specifications used in the current study, this value is ~ 40 μm. A direct implication of this result is that as long the fault severity is less than ~ 40 μm, the pump performance will stay put even under extreme conditions, where all nine of its cylinders have leakage fault. Therefore, $h \leq 40\ \mu m$ represents a healthy pump. Second, beyond this threshold, the number of faulty cylinders that the pump can bear without a drop in its performance depends on the severity of the leakage fault. For instance, at ~ 40 μm and below, the pump can remain healthy with leakage fault in 5 – 9 cylinders. With increase in faulty severity to ~ 50 μm, the pump can maintain healthy operation with up to 3 - 4 faulty cylinders, which drops to two faulty cylinders at ~ 60 μm, and just one faulty cylinder at ~ 70 μm. With any further increase in the fault severity, the pump cannot afford even a single faulty cylinder to maintain the output flow rate within the range of healthy operation (less than 5% drop in the delivery flow rate: see green dotted line Fig. 5.6 (a). Conversely, we can say that for a given number of faulty cylinders, there is a corresponding maximum value of fault severity beyond which the outlet flow rate drops below the healthy operational range of the pump. Recall the discussion from section 5.2.1.1. for a single faulty cylinder, the pump's condition was defined based on the severity of leakage fault (h) as healthy ($h \leq 40$ μm), moderately faulty (40 μm $< h <$ 80 μm) or severely faulty ($h \geq 80$ μm). In the case of multiple faulty cylinders, the pump's condition under these three categories varies with the number of faulty cylinders, as detailed in Table 5.1.

Table 5.1: The range of fault severity that determines the pump's condition corresponding to the number of faulty cylinders. Note that the range of fault severity for moderately faulty conditions reduces with increasing number of faulty cylinders and vanishes for five or more faulty cylinders.

No. of faulty cylinders	**Pump condition**	**Healthy**	**Moderately faulty**	**Severely faulty**
1		$h \leq 40$ µm	40 µm $< h <$ 80 µm	$h \geq 80$ µm
2		$h \leq 40$ µm	40 µm $< h <$ 60 µm	$h \geq 60$ µm
3		$h \leq 40$ µm	40 µm $< h <$ 50 µm	$h \geq 50$ µm
4		$h \leq 40$ µm	40 µm $< h <$ 50 µm	$h \geq 50$ µm
5		$h \leq 40$ µm	-	$h > 40$ µm
6		$h \leq 40$ µm	-	$h > 40$ µm
7		$h \leq 40$ µm	-	$h > 40$ µm
8		$h \leq 40$ µm	-	$h > 40$ µm
9		$h \leq 40$ µm	-	$h > 40$ µm

At the top of Fig. 5.6, the maximum value of fault severity is represented by the horizontal bar's length for each number of faulty cylinders. The trend of these horizontal bars shows that while the value of faulty severity that permits healthy pump operation decreases with increasing number of faulty pistons, this trend is not linear. After a certain number of cylinders get damaged (in the present case, five or more out of nine cylinders), the fault severity that allows healthy operation reaches its limiting value of ~ 40 μm. The fault severity saturates to a limiting value because five or more faulty cylinders in the pump means that at any instant in time, the discharge port will have at least one faulty cylinder traversing it, which is not the case for less than five faulty cylinders.

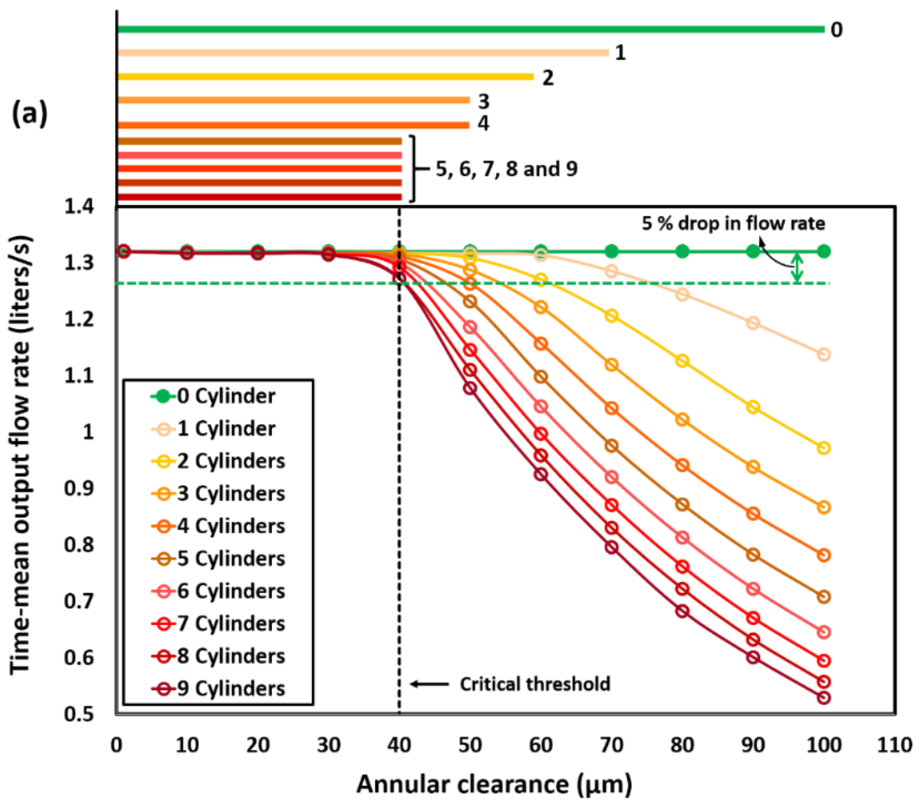
(a)
0
1
2
3
4
5, 6, 7, 8 and 9
5 % drop in flow rate
Critical threshold
0 Cylinder
1 Cylinder
2 Cylinders
3 Cylinders
4 Cylinders
5 Cylinders
6 Cylinders
7 Cylinders
8 Cylinders
9 Cylinders
Time-mean output flow rate (liters/s)
Annular clearance (µm)

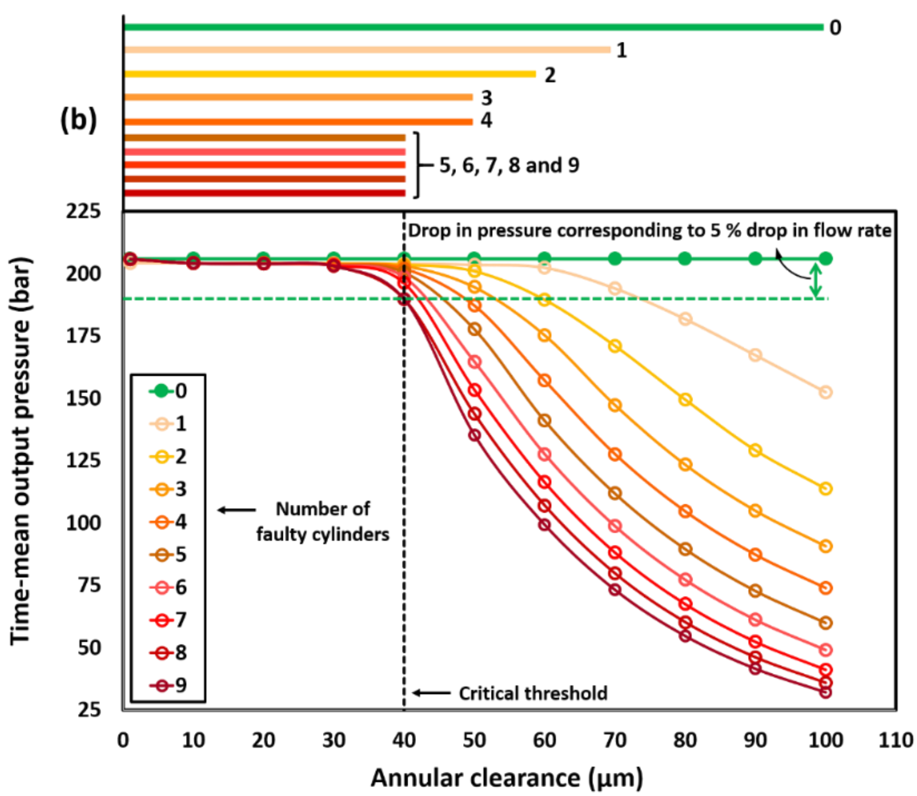
(b)
0
1
2
3
4
5, 6, 7, 8 and 9
Drop in pressure corresponding to 5 % drop in flow rate
Number of faulty cylinders
Critical threshold
Time-mean output pressure (bar)
Annular clearance (µm)

Fig. 5.6: Time-mean response of (a) flow rate, and (b) pressure at the pump outlet as a function of severity of leakage fault and the number of faulty cylinders.

5.2.3. APP's health detection through FFT analysis

5.2.3.1. Single cylinder fault detection

In section 5.2.1, it was demonstrated that besides the reduction in the time-mean magnitude of the outlet pressure and flow rate, the temporal signature of the dynamic pressure and flow rate waveform also changes with increasing wear. This effect can be captured by the frequency responses of the time-varying signals, as shown in Fig. 5.7. The characteristic frequencies observed in the FFT spectra are due to the following operational aspects of the pump:

a. Rotational frequency: This corresponds to the rotational speed of the pump (2500 rpm or 41.67 rps), which is $X = 41.67$ Hz.

b. Pump discharge frequency (f): This is a characteristic frequency of the discharge flow at the pump outlet and appears in the frequency response regardless of the pump condition. If N_p is number of pistons in the pump, the pump discharge frequency (f) is calculated as:

$$f = N_p \times X = 9 \times 41.67 = 375 \text{ Hz} \tag{5.1}$$

c. Pump discharge frequency sidebands ($f - X, f + X$): The frequency sidebands appear in frequency response around the pump discharge frequency (f) as the centre and are equidistant from it, *i.e.*, $f - X$ and $f + X$. The frequency sidebands occur due to the modulation of the pump discharge frequency by the rotational frequency (X), where the carrier frequency is the pump discharge frequency f, and the modulating frequency is the rotational frequency X.

Fig. 5.7 shows the frequency spectra of the pump outlet pressure for different levels of leakage fault severity in a single cylinder. In each spectrum, the peaks can be observed at the pump discharge frequency (f), and its super-harmonics: $2f, 3f, 4f$ *and* $5f$. Figures 5.7 (a-c) present the frequency responses for stage I ($h \leq 40$ µm) for three representative cases *i.e.*, a healthy pump, 10 µm and 30 µm. The dominant frequency peak appears at the rotational frequency X, the pump discharge frequency f (375 Hz), and other major peaks appear at the second (750 Hz) and the third harmonic (1125 Hz) of f. Apart from these frequency peaks, the sidebands appear around frequency f and its super harmonics, which are most significant around f, $2f$ and $3f$. The frequency response for Stage II (40 µm $< h <$ 80 µm) is shown in Figures 5.7 (d-f). In stage II, the dominant frequency peaks appear at f, $2f$ and $3f$ (see Fig. 5.7 (d-e)), and the amplitude corresponding to the frequency f and its sidebands increases with increasing severity of leakage fault. Note that as the fault severity increases to 60 µm, in addition to the peaks at $f, 2f$ and $3f$, the dominant peak also starts appearing at the rotational frequency X. In the extreme condition, as the fault severity increases significantly, corresponding to stage III ($h >$ 80 µm), the peak amplitude appears at the rotational frequency (X) and its harmonics (see Figures 5.7 (g-h)). This indicates that in stage II, as the fault severity increases, the amplitude of f and its sidebands increases until a critical value of fault severity is reached, after which the dominant peak shifts from the pump's discharge frequency and its sidebands to the pump's rotational frequency X and its super harmonics (2X and 3X). At this critical value of fault severity, the ratio of amplitudes of X and f *i.e.*, ratio $\epsilon =$ (amplitude (X) /amplitude (f)) becomes greater than or equal to unity ($\epsilon \geq 1$). This marks the onset of stage III ($h >$ 80 µm) and corroborates the observation of section 4.2.1.1. that a critical threshold value of leakage fault severity exists beyond which the pump output pressure decays significantly. Therefore, if the peak amplitude occurs at the rotational frequency (X), and its amplitude is greater than the amplitude f, it can be inferred that the pump is operating under a faulty condition. Further, the larger their ratio (ϵ) the larger is the faulty severity. Furthermore, if in addition to X, the dominant peaks also appear at the super harmonics of the rotational frequency (X) *i.e.*, $2X$ and $3X$, it can be inferred that the pump is operating under a severely faulty condition. Based on the ratio $\epsilon =$ (amplitude (X) /amplitude (f)), the pump's condition can be identified as follows:

Healthy: $\epsilon < 1$

Moderately faulty: $\epsilon \to 1$

Severely faulty: $\epsilon \gg 1$

The fact that dominant frequencies appear in the frequency spectra at the pump discharge frequency (f) and its harmonics for both healthy and faulty conditions indicates that they are inherent to the pump's operation. Therefore, any deviation from these frequencies or appearance of dominant frequencies at rotational frequency (X) and its harmonics can be attributed solely to piston wear.

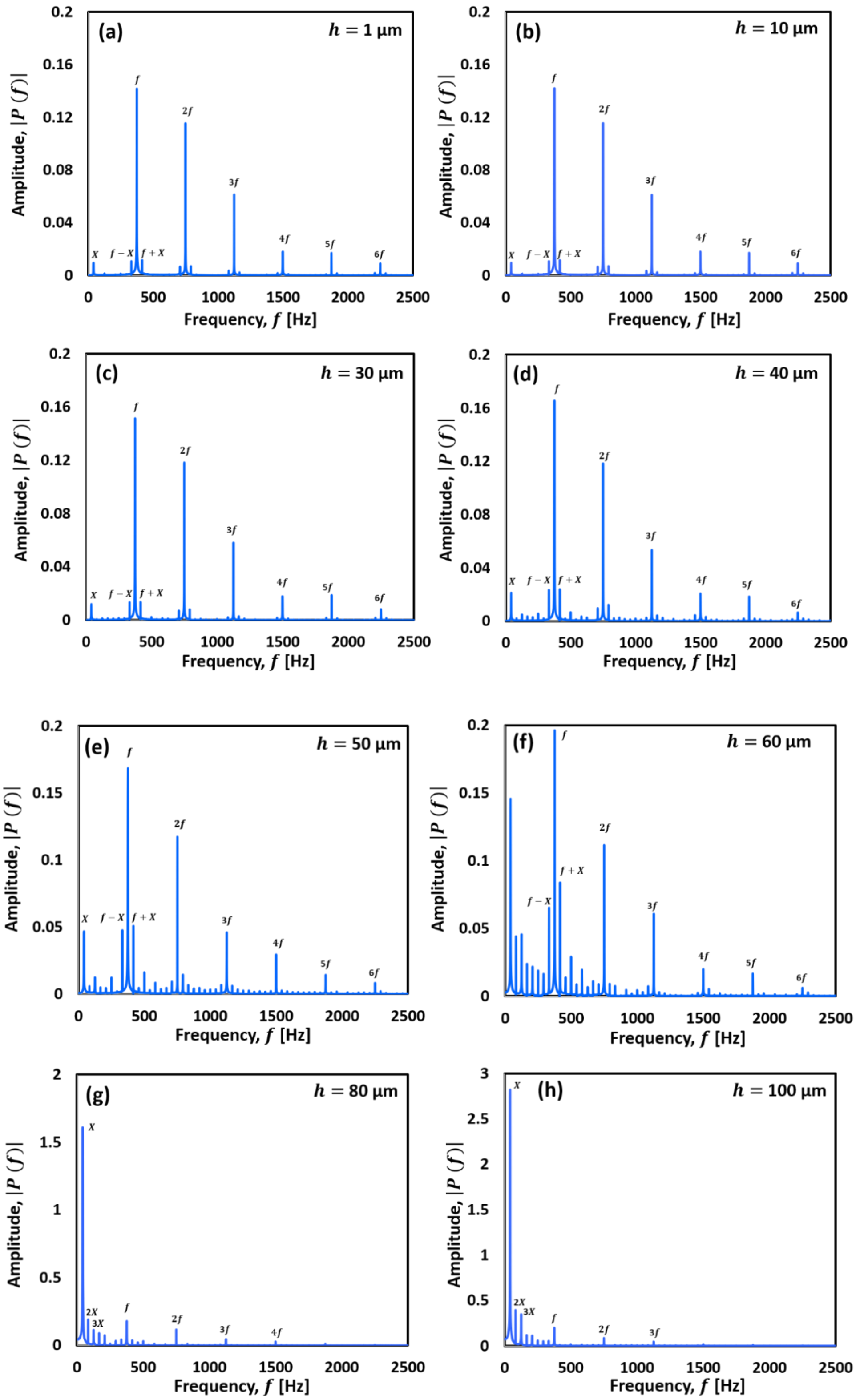
(a)
$h = 1$ μm
(b)
$h = 10$ μm
(c)
$h = 30$ μm
(d)
$h = 40$ μm
(e)
$h = 50$ μm
(f)
$h = 60$ μm
(g)
$h = 80$ μm
(h)
$h = 100$ μm
Amplitude, $|P(f)|$
Frequency, f [Hz]
X
$f - X$
$f + X$
f
$2f$
$3f$
$4f$
$5f$
$6f$
$2X$
$3X$

Fig. 5.7: FFT spectra at different levels of leakage fault severity: (a) $h = 1$ µm, (b) $h = 10$ µm, (c) $h = 30$ µm, (d) $h = 40$ µm, (e) $h = 50$ µm, (f) $h = 60$ µm, (g) $h = 80$ µm, and (h) $h = 100$ µm.

In addition to calculating the ratio ϵ, the trend of the amplitude of the side-band frequencies of f can be used to detect and assess the severity of leakage fault. Specifically, the variation of ratios of amplitudes of the pump's discharge frequency to the amplitude of its sideband frequencies is given by:

$$R_1 = \frac{amplitude\ (f)}{amplitude\ (f-X)} \quad (5.2)$$

$$R_2 = \frac{amplitude\ (f)}{amplitude\ (f+X)} \quad (5.3)$$

The variation of R_1 and R_2 as a function of the severity of leakage, the fault is shown in Fig. 5.8, which indicates that as the fault severity increases, the rate at which the amplitude of sideband frequencies increases is more than that of the pump discharge frequency (f), which is center frequency. A decrease sees this in the magnitude of R_1 and R_2. The magnitude of these ratios decreases to approximately 50 µm, then stagnates from ~ *h*= 50 - 80 µm, and then increases beyond 80 µm. The appearance of three separate sections of the fault severity in the trend of R_1 and R_2 align with the three conditions of the pump as discussed in section 5.2.1.1. Further, the increase in the value of R_1 and R_2 beyond $h = 80$ µm indicates that this is a critical threshold, after which the pump's condition deteriorates drastically. Therefore, ratios R_1 and R_2 are important indicators of the fault severity, and their trends can help assess the health condition of an axial piston pump.

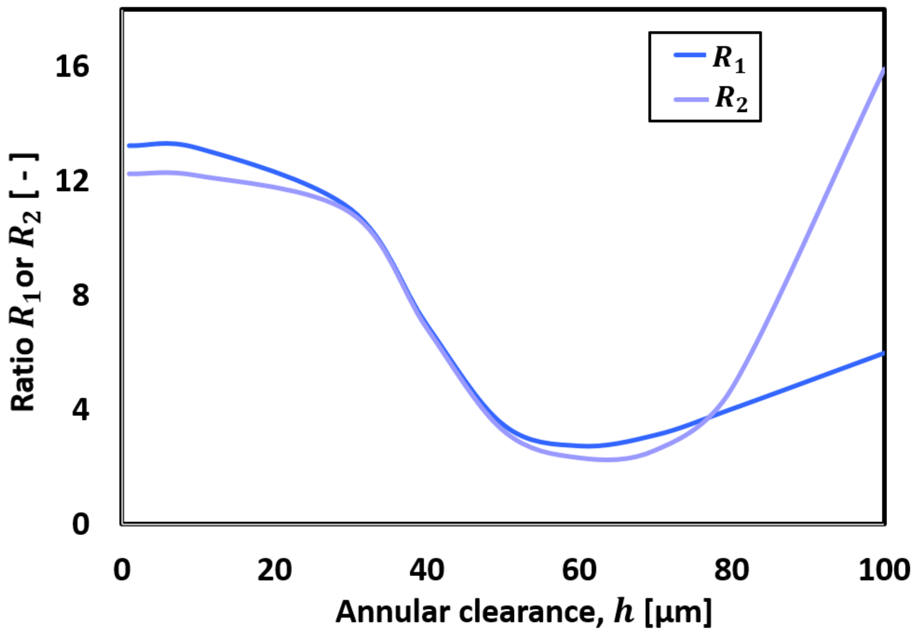

Fig. 5.8: Variation of the parameters R_1 (Eq. 26) and R_2 (Eq. 27) with the severity of leakage fault.

5.2.3.2. Multiple cylinder's fault detections

Unlike in the case of a single faulty cylinder, the fault parameters R_1 and R_2 do not exhibit a specific trend for multiple faulty cylinders. Instead, the ratio $\epsilon =$ (amplitude (X) / amplitude (f)) is a better indicator that displays the same trend as that of a single faulty cylinder. Specifically, for up to eight faulty cylinders, the pump's condition can still be demarcated as either healthy or moderately faulty or severely faulty for $\epsilon < 1$, $\epsilon \to 1$, and $\epsilon \gg 1$, respectively. Further, the value of ϵ increases with the increasing severity of leakage fault, which is the same as that observed for a single faulty cylinder. However, the extreme case of nine faulty cylinders represents a unique pump condition, where all its cylinders are faulty. In this condition, the ratio is found to be $\epsilon \gg 1$. Since the fault in multiple cylinders also leads to a noticeable drop in the time-mean value of the flow parameters (flow rate and pressure) at the pump outlet (section 5.2.1.2), the leakage fault can be diagnosed reliably by determining the value ratio ϵ as well as considering the time-mean value of the flow parameters simultaneously.

5.3. Summary

This chapter uses a mathematical model-based simulation technique to evaluate the effect of increasing the severity of a leaking fault (growing the annular gap) on pump performance in both single and multiple cylinders simultaneously. The leakage is represented by laminar flow across the uniform annular gap between the piston and cylinder. It also displays time-varying pressure signals for six sample fault severity levels ($h = 1$ µm, 30 µm, 40 µm, 50 µm, 60 µm, and 80 µm). With a single defective cylinder, when the wear (annular gap) rises, the pump's time-mean outlet flow and pressure remain constant until a critical threshold, then suddenly decrease, resulting in a decrease in the pump's volumetric efficiency. With the increase in faulty cylinders this critical threshold shifts to lower magnitudes, and in the limit of more than four faulty cylinders, this threshold saturates to a constant magnitude. Furthermore, the enhanced form of the leaking defect in multiple piston-cylinders with many different conceivable arrangements of faulty pistons is discussed in the next chapter.

Moreover, the dynamic signal's data show that the increasing severity of leakage and the increasing number of faulty cylinders modulate both the time signature and the amplitude fluctuations of the outlet pressure waveform due to the reduced flow in the discharge cycle. Further, FFT analysis of these dynamic signals and the time-mean value of pressure and flow rate leakage fault diagnosis is presented to classify the pump's condition as either healthy, moderately faulty, or severely faulty.

Chapter 6

Arrangement of leakage faulty pistons

6.1. Introduction

This chapter proposes a methodology for identifying defective pistons' best (optimal) geometrical configurations (in section 6.3), resulting in minimum peak-to-peak pressure fluctuations at the outlet of an internally leaking APP. This method would allow the pump to operate at the least pressure fluctuations and vibrations at its outlet, furthermore by categorizing the various piston configurations based on their dynamics of net pressure responses using a model-based study. So, the Hydraulic industry can benefit from this technique in terms of cost and reusability of the pump. The significant benefits of this proposed solution can be followed as follows:

1. By continuously reusing defective pumps and extending the pump's operating cycle.

2. A damaged piston may be overused to its maximum potential by reducing the pump's internal vibrational effects resulting from each defective piston, allowing it to perform at its best even under a damaged condition.

3. Reduced maintenance costs and simplicity of usage can significantly improve the pump's dependability.

4. Axial-piston pumps can be made more efficient or flexible, and their noise and costs can be reduced when various alternative configurations are implemented within a malfunctioning pump.

6.2. Methodology

As the faulty piston bore rotates from suction to discharge side, nonuniform pressure fluctuations (or ripples) in the piston bore cause vibration and

FBNs to occur. Although the time means value of net discharge pressure and flow were constant, their peak-to-peak value varies. Therefore, this study attempts to minimize the peak-to-peak fluctuations later by modifying the geometric configurations of defective pistons inside the barrel. To keep pressure ripples as minimal as feasible, these several potential configurations aim to distribute fault piston severity inside the pump evenly.

To further demonstrate the methodology for analyzing the various piston-cylinder layouts in this research, see Figure 6.1.

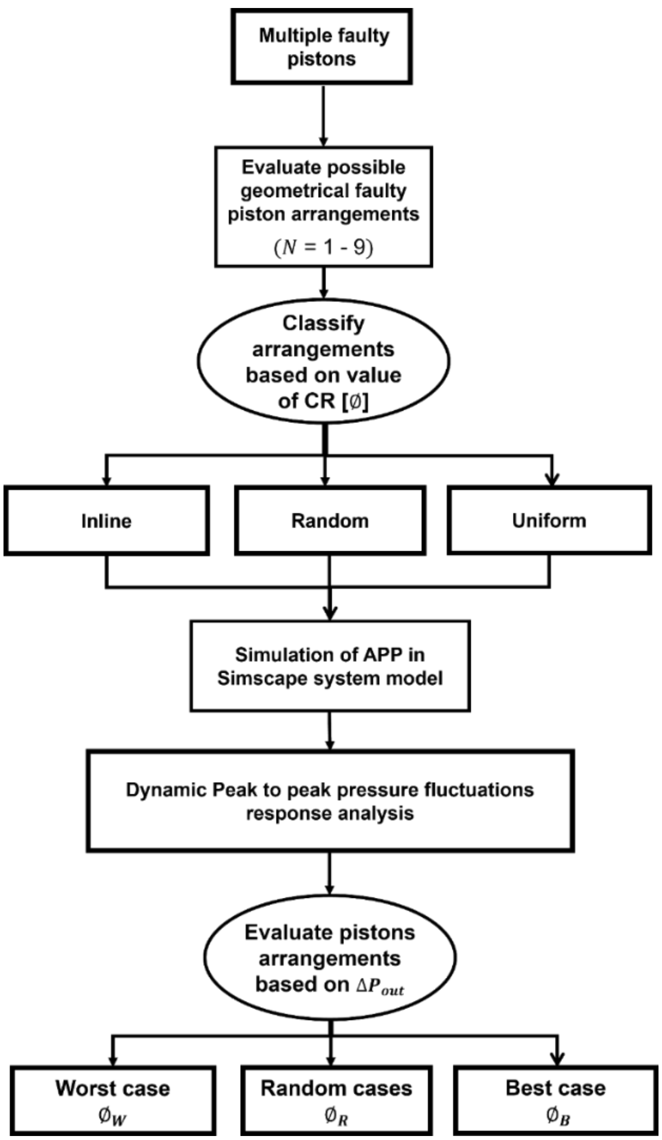

Fig. 6.1: Applied methodology to evaluate the configuration of the piston

Further down in this chapter, the piston-cylinder leakage fault in multiple cylinders simultaneously is discussed. Hence, many potential configurations for faulty pistons have been found based on the number of defective pistons (N) occurring concurrently within the cylinder barrel. For better visualization of the study, Figure 6.2 shows the exploded view of APP along with the annular leakage region and showcases the different possible arrangements of faulty pistons (N; e.g., Only for $N = 3$ as shown in Fig. 6.2) as all healthy, inline, random, uniform, and all faulty arrangements. To further understand the concept of all possible arrangements, consider the example of $N = 3$ defective pistons for all types of conceivable arrangements.

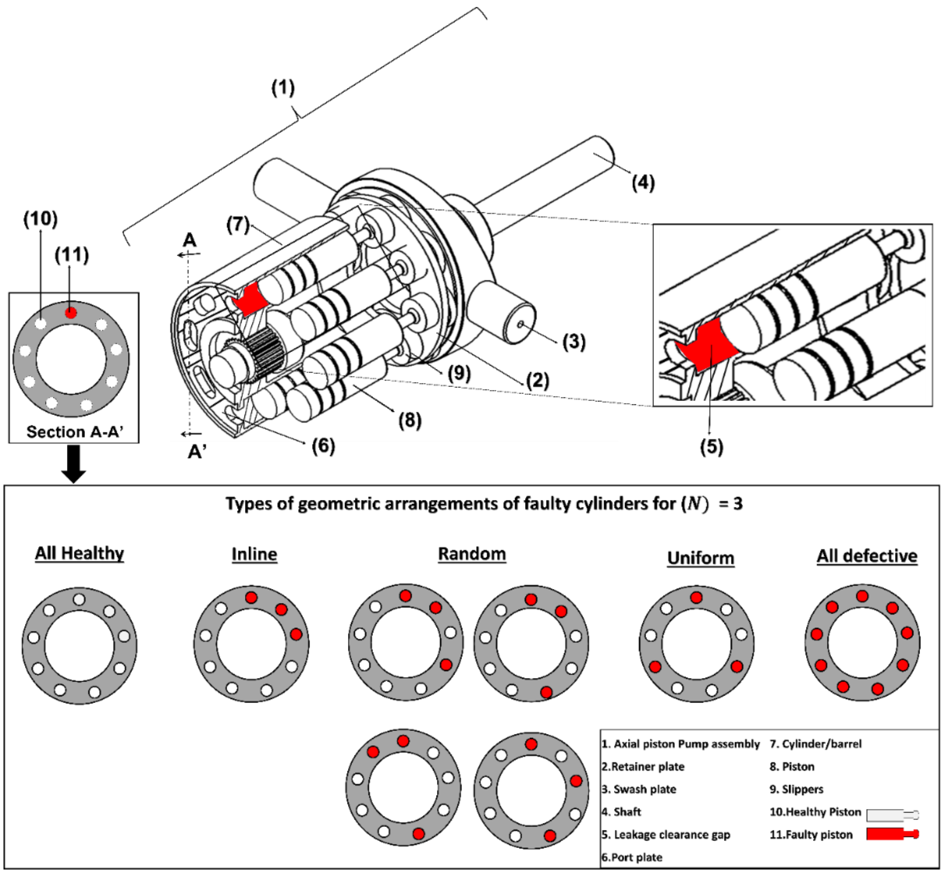

Fig. 6.2: Exploded view of axial piston pump (APP), followed by subdivision of piston arrangements such as: All healthy, inline, random, uniform, and all defective respectively for pistons fault severity of $N = 3$.

To compare these various geometric configurations, as shown in Fig. 6.3 a variable known as the configuration ratio (CR): $\emptyset$is derived, which is defined as the ratio of linear distance (L_S) between two faulty cylinders to the maximum linear distance (L_{max}) between two faulty cylinders for $N < 3$ only. And for $N \geq 3$, CR is defined as the shaded portion's area (A_S) formed by joining the center of each defective piston to the area of a cylinder's circular face (A_C). However, due to the unique arrangement of $N =$ (0, 1) and 9, this CR value is zero and unity, respectively, as shown in Eq. 6,1.

$$\emptyset = \left| \begin{array}{cc} \mathbf{0} & N = 0, 1 \\ \dfrac{\boldsymbol{L_s}}{\boldsymbol{L_{max}}} & N = 2 \\ \dfrac{\boldsymbol{A_s}}{\boldsymbol{A_c}} & 3 \leq N \leq 8 \\ \mathbf{1} & N = 9 \end{array} \right| \forall [0 \;\; 1] \qquad (6.1)$$

6.3. Arrangements

Figure 6.3 depicts all conceivable geometrical configurations for the various arrangements (inline, random, and uniform) and the number of faulty pistons (N), with the increasing number of faulty pistons shown from top to bottom. For the number of faulty pistons (N), these arrangements are classified as **1.** inline, **2.** random, and **3.** uniform, and then further into type A (top two rows for $N < 3$) and type B (bottom rows for $N \geq 3$) severity based on the definition of CR ($\emptyset$), as stated in Eq. 6.1. In type A, the linear distance (L_s and L_{max}) between two defective pistons are used to classify the arrangements, but in type B, the areas joining faulty pistons (A_S and A_C) are utilized to classify the arrangements. The length (L_S) and shaded area (A_S) is determined for each number of defective pistons (N=1 to 9) using the method of n-sided irregular closed polygon, as demonstrated briefly in appendix-A.

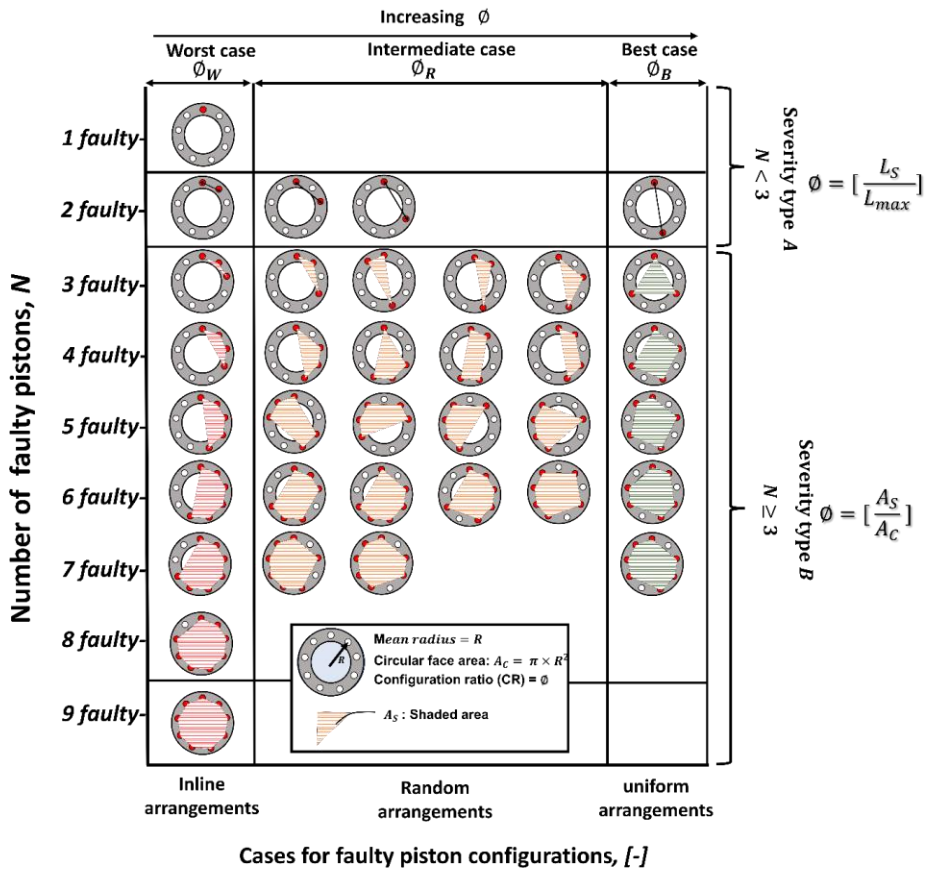

Fig. 6.3: Illustrates all possible geometrical arrangements of faulty pistons classification under the different levels of piston faults severity $N \in [1 - 9]$.

Table. 6.1 shows the values of CR that always fall between 0 (which denotes $L_s = 0$) and 1 (denotes $L_s \approx L_{max}$ or $A_s \approx A_c$). Further, the value CR = 0 and 1 physically reflect all healthy pistons ($N = 0$) and all faulty pistons ($N = 9$) inside the barrel of APP, respectively. However, all the values are calculated for ∅ each type of arrangement using mentioned formulae in Eq. 6.1, as shown in Table. 6.1. In reference to Fig. A.1 and table. 6.1, when N lies between $3 \leq N \leq 8$, both the areas A_S and A_C tend to have non-zero values, and therefore, the ratio ∅ lies between 0 and 1 and as ∅→1 represents the most uniform configuration corresponds to each value of N. Further in Fig. 6.3, the last row of piston arrangements shows that the number of defective pistons is significantly greater for N = 9, so the number of feasible geometrical configurations is unique, and thus no other arrangement is available other than inline type and corresponds to that the value of CR is unity ($A_s \approx A_c$).

Table 6.1: Theoretical value of CR ($\emptyset$) corresponds to the value of each N and pistons arrangements

N \ ϕ	Inline arrangement	Random arrangement				Uniform arrangement
1 faulty	0	0	0	0	0	0
2 faulty	0.347	0.499	0.879	-	-	1
3 faulty	0.048	0.140	0.211	0.211	0.259	0.414
4 faulty	0.169	0.307	0.397	0.470	0.470	0.608
5 faulty	0.355	0.518	0.519	0.582	0.589	0.729
6 faulty	0.566	0.704	0.704	0.704	0.777	0.777
7 faulty	0.751	0.822	0.823	-	-	0.825
8 faulty	0.872	-	-	-	-	-
9 faulty	1	-	-	-	-	-

[-] piston arrangements does not exists

After considering all possible configurations for the relevant piston faults (N) in this section, the effects of all potential faulty piston configurations on pump performance must be thoroughly examined in the next section of this chapter 6 (results and discussion), followed by the APP system modelling and dynamic peak to peak pressure response analysis.

6.4. Results and Discussion

The current disclosure presents a troubleshooting approach; the primary goal is to suppress the pump's vibrational effect (peak-to-peak fluctuations) and decrease maintenance costs by boosting the performance of an old/faulty pump merely by adjusting the arrangement of faulty pistons within the axial piston pump. As a result, the geometric configurations shown in figure 6.3 are further classified in this section based on their peak-to-peak pressure amplitude variations at a pump output (shown in Fig. 6.4) as follows:

$$\begin{aligned} &\textbf{Worst configuration:} && \emptyset_W \\ &\textbf{Intermediate configuration:} && \emptyset_R \\ &\textbf{Best configuration:} && \emptyset_B \end{aligned} \tag{6.2}$$

Further, Figure 6.4 depicts the peak-to-peak pressure fluctuations on the ordinate and the number of faulty pistons on the abscissa (N= 1 to 9) at the pump discharge. These curves have been obtained from the simulation of the APP hydraulic system model (as shown in chapter 4). This hydraulic simulation is performed to investigate the influence of different degrees of leakage gap (h) between the piston-cylinder, namely as 20 μm (small gap), 60 μm (medium gap), and 100 μm (large gap) on the peak-to-peak pressure amplitude (ΔP_{out}) at the pump's outlet. Fig. 6.4 showcases the effect of multiple pistons fault, with the worst configurations representing the maximum peak-to-peak pressure amplitude ($\Delta P_{out,\ max}$) and the best configurations representing the minimum peak-to-peak pressure amplitude ($\Delta P_{out,\ min}$), with the rest of the intermediate configurations lie between these two extreme cases (worst and best) for a given value of N and h.

As a result, Fig. 6.4 (a), at a leakage gap of $h\ = 20\ \mu m$, the ΔP_{out} exhibits negligible variations regarding the number of piston defects (N) and configurations ($\emptyset$), which vary within a limited range of 5-10 MPa while maintaining a constant net mean pressure of 20.5 MPa at the pump discharge. As a result, it is concluded that the low degree of leakage gaps in APP piston-cylinders does not influence pump performance regardless of configuration.

Further, Fig. 6.4 (b, c) shows the medium and large leakage gap conditions ($h = 60$ and $100\ \mu m$), respectively. It can be seen in both ig. 6.4 (b, c) that for each value of *N*, the maximum points of peak-to-peak pressure fluctuation are simulated as corresponding to the worst configuration and the minimum points as corresponding to the best configuration, with the rest of the fluctuations considered as intermediate configurations.

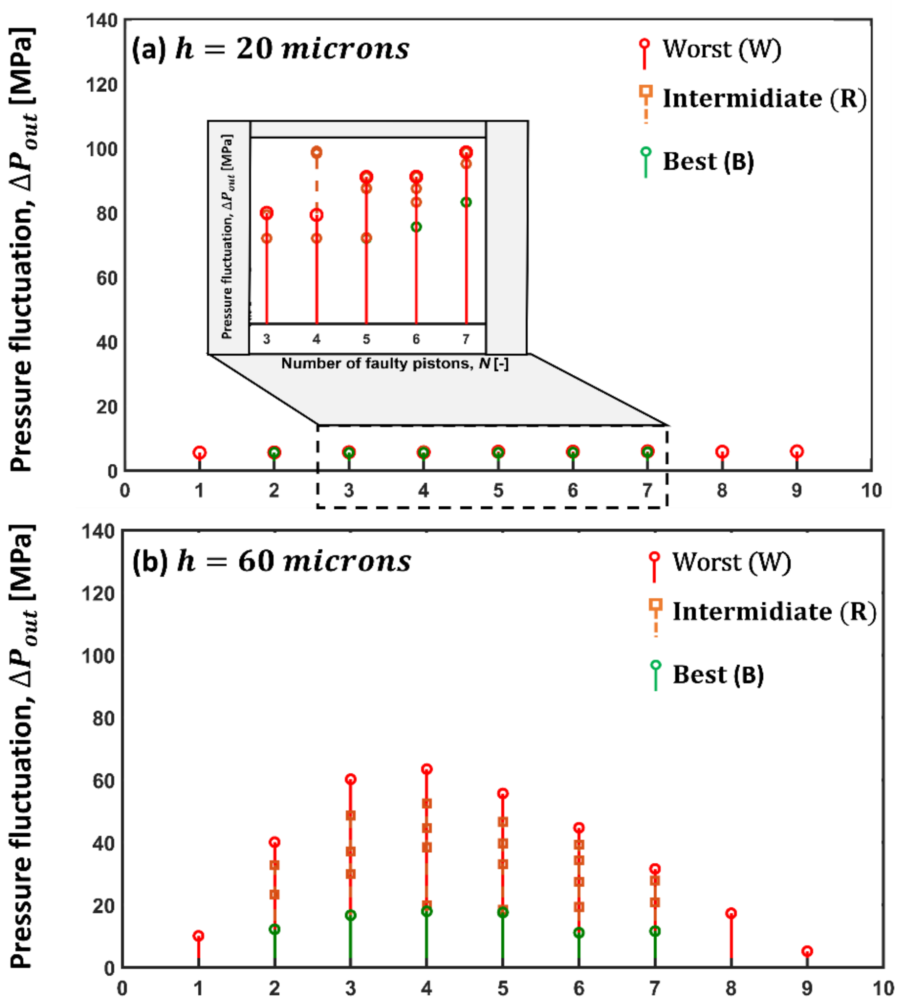

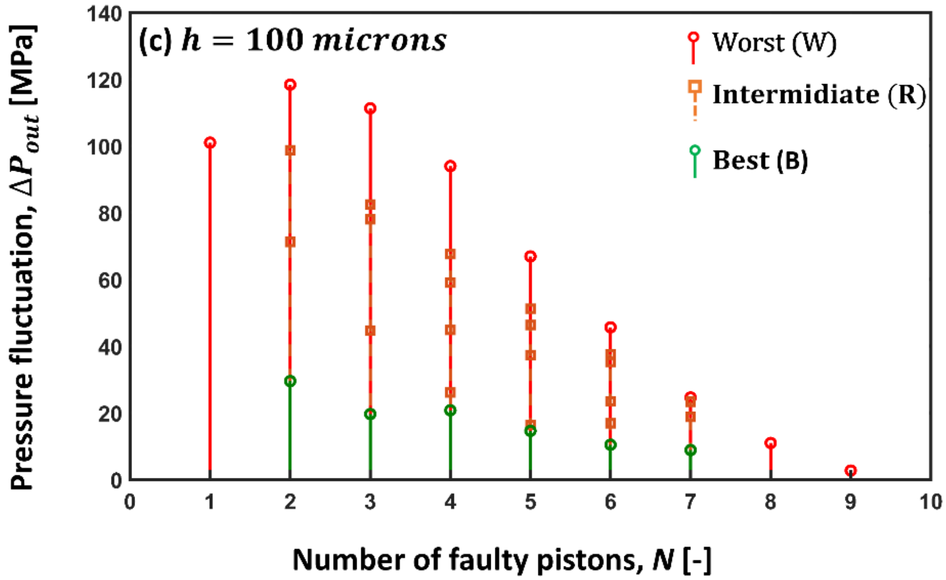

Fig. 6.4: Plots for a peak-to-peak amplitude for the respective number of pistons faults correspond to different (worst (W), intermediate (R) and best (B) cases); (a) $h = 20$ µm, (b) $h = 60$ µm, (c) $h = 100$ µm.

Figure 6.5, to support the worst, random, and best configurations for better visualization of pressure fluctuations with signals charts over 0.125 seconds (4 pump cycles, 0.2544 sec) for the value of N = 2 and leakage gaps ($h = 20, 60$, and 100 μm), the worst to best configurations can also be illustrated by dynamic (temporal) signals of the net pressure at the pump outlet (or discharge) respectively.

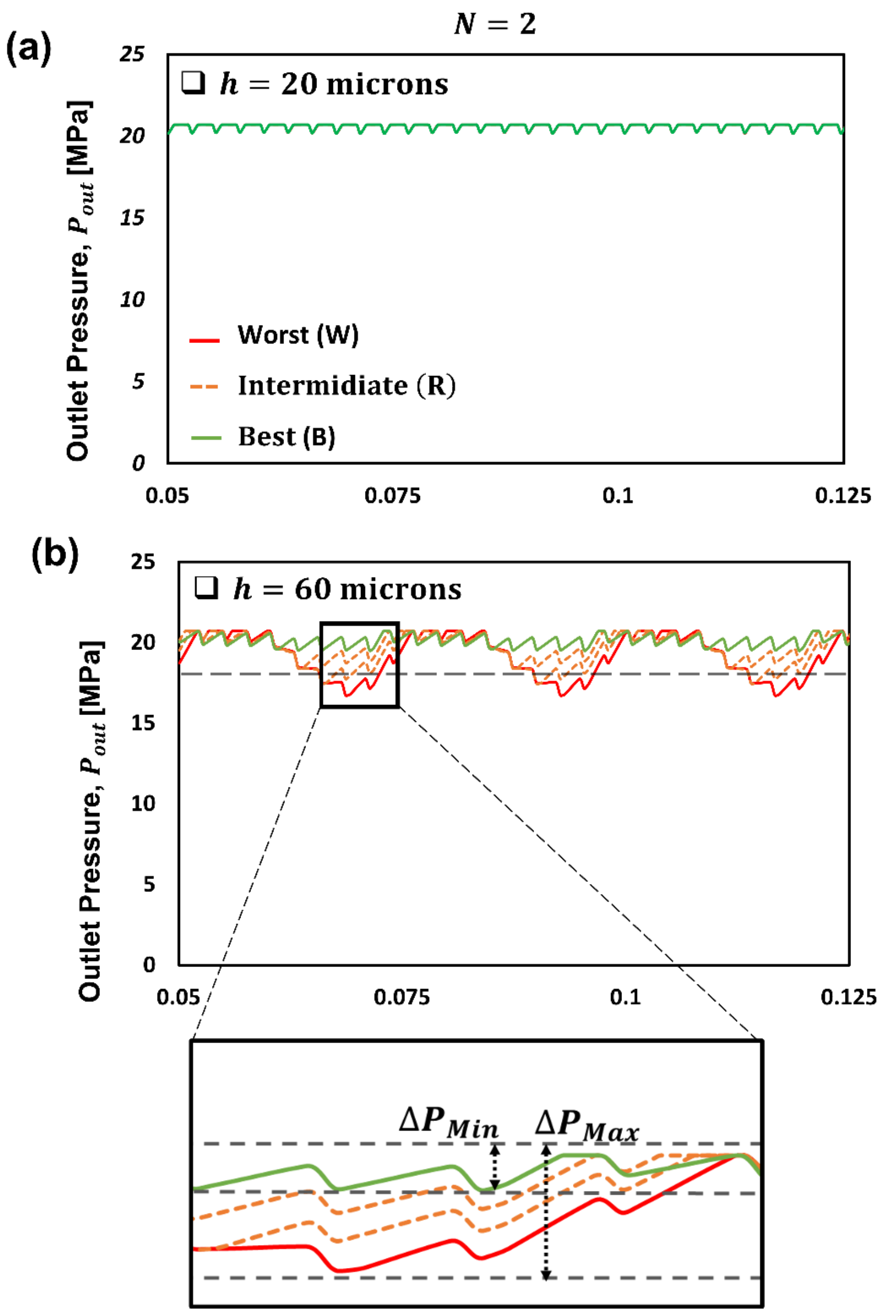

$N = 2$
(a)
$h = 20$ microns
Outlet Pressure, P_{out} [MPa]
25
20
15
10
5
0
0.05
0.075
0.1
0.125
Worst (W)
Intermidiate (R)
Best (B)
(b)
$h = 60$ microns
Outlet Pressure, P_{out} [MPa]
25
20
15
10
5
0
0.05
0.075
0.1
0.125
ΔP_{Min}
ΔP_{Max}

(c)

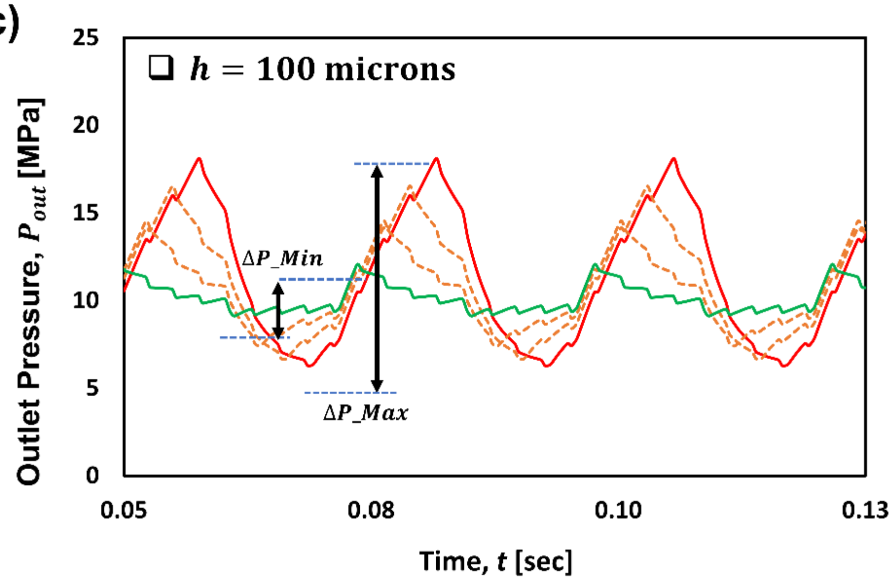

Fig. 6.5: Temporal variation of the net pressure at the pump outlet with the number of faulty Pistons; $N = 2$ **(a-c)** at different levels of leakage severity: h = 20, 60, and 100 μm respectively.

The effect of undesirable FBNs within the axial pump is highly influenced by the degree of leakage (h) and defective pistons (N), as seen in figures 6.4 and 6.5. Several previous studies on axial piston pumps indicate that their performance is primarily governed by two critical parameters: the degree of annular gap and the number of defective pistons. However, the pump performance is now also affected by the configuration of the faulty pistons within an APP. In terms of the magnitude of ΔP_{out}, there are a specific number of configurations of defective pistons labeled as **worst, intermediate,** and **best** for each value of N. As a result of this peak-to-peak pressure amplitude, the optimal configurations across all values of N can be evaluated, which possess the least fluctuations and vibrations within the axial piston pumps.

6.5. Summary

When using an APP, there is a possibility of wear (internal leakage) occurring in multiple pistons-cylinders simultaneously. In the event of multiple pistons failing, inline arrangements are the ideal but not best configuration layout of defective pistons for mitigating peak-to-peak fluctuations during pump discharge. In such faulty pump conditions, the pressure and flow variation create vibrations, which can cause premature failure of pump components. So, when it comes to finding out which configuration of defective pistons would result in the lowest peak-to-peak pressure variations under internal leakage at APP's outlet, a model simulation and analytical technique have been proposed in this chapter.

If there are just two defectives' pistons (N =2), then the optimum configuration is the one with the pistons situated on diametrically opposite ends. If there are three or more defective pistons ($N \geq 3$), the optimal configurations correspond to $\max \mathrm{CR}\,(\phi) \rightarrow \phi_B$ with maximum area enclosed (A_S) by the joining defective pistons. The amplitude waveforms of dynamic signals varied in response to each leakage fault (20 μm, 60 μm, and 100 μm), allowing researchers to visualize the increasing severity of a leakage fault (h) as well as the many possible configurations for defective pistons (N). For the number of defective piston configurations (N) corresponding to various leakage severities, the dynamic pressure data is utilised to classify the pump's condition as worst-case, slightly intermediate, or best-case (h).

Chapter 7

Conclusion and Scope of Future work

7.1. Introduction

The Simulink (Simscape) model is built on the MATLAB 2020b platform to examine the optimum performance of the axial piston pump and its parameters based on the different number of faulty pistons corresponding to different leakage severity. The current study or approach additionally fulfills the stated goal by offering a way to monitor the condition of an axial piston pump. And within the axial piston pump, the healthy and faulty pistons are recognized.

The following thesis will conclude the overall research findings in two sections, 7.2 and 7.3.

7.2. Leakage fault severity in single and multiple cylinders

This section of this research study presents a simulation and model-based approach to simulate the growing severity of leakage fault (increasing annular gap) in both single and multiple cylinders simultaneously on the pump performance. The pump's performance (in terms of its volumetric efficiency) varies non-linearly with the leakage fault parameters.

1. For a single faulty cylinder, the flow rate and pressure at the pump discharge remain constant up to a certain value (first threshold) of the fault severity, then decrease slowly. A critical threshold (second threshold) is reached with a further increase in fault severity, beyond which they decrease drastically.
2. In multiple faulty cylinders, with the increasing number of faulty cylinders, this critical threshold (the second threshold) reduces to lower

magnitudes, and in the limit of more than four faulty cylinders saturates to the value equal to that of the first threshold.

3. This demonstrates that more than four faulty cylinders are a limiting condition for the pump where one faulty cylinder is always present in the discharge cycle. In this condition, the pump is restricted to the maximum possible value of fault severity that it can bear, *i.e.*, it can stay in the healthy condition and perform efficiently only below this value.

Overall, the combined effect of the severity of leakage fault and the number of faulty cylinders on the pump performance can be visualized through the 3D plot in Fig. 7.1, which shows the volumetric efficiency ($\eta_{vol} = Q_{net,actual} / Q_{net,theoretical}$) of the axial piston pump as a function of these fault parameters.

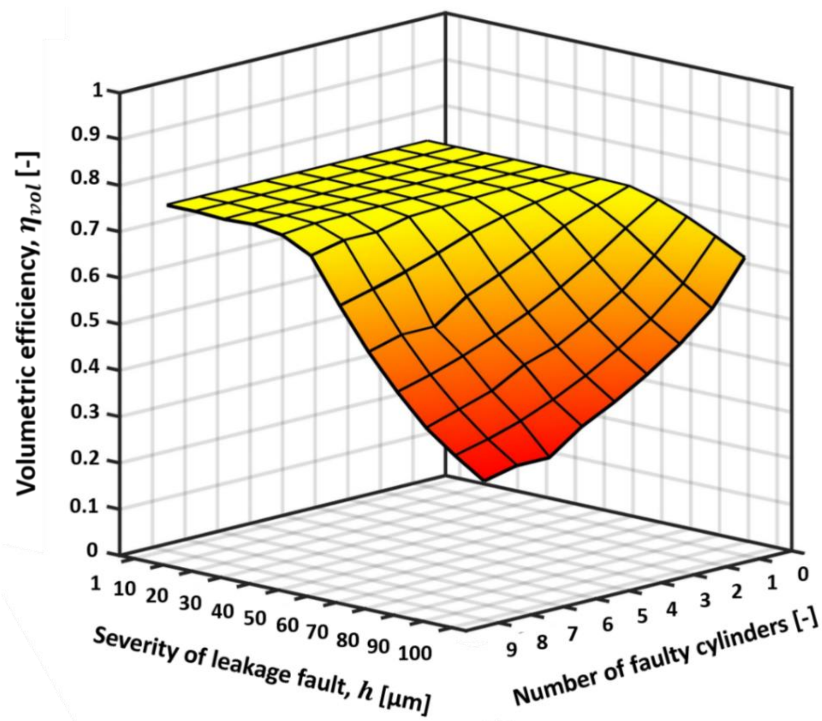

Fig. 7.1: Variation of volumetric efficiency of a pump with increasing severity of leakage fault and number of faulty cylinders

A FFT analysis of the time-varying pressure signals at the pump outlet indicates that the deterioration in the pump's performance can be tracked by comparing the amplitudes of the frequency peak at the rotational frequency and the pump's discharge frequency.

1. For up to eight faulty cylinders, the ratio of amplitudes of these frequencies $\epsilon =$ (amplitude (X) / amplitude (f)) is $\epsilon < 1$ for healthy conditions, $\epsilon \rightarrow 1$ for moderately faulty conditions, and $\epsilon >>1$ for a severely faulty condition.
2. In the extreme case of all faulty cylinders (all nine cylinders), the ratio ϵ is << 1, and the time-mean flow rate and the pressure at the pump outlet drop to significantly low magnitudes.

This way, based on relative amplitudes of the peak at the rotational frequency and the pump's discharge frequency in the FFT spectra, and the time-mean value of flow parameters (flow rate and pressure), the pump’s health condition w.r.t leakage fault can be detected, and the pump's condition can be demarcated as either healthy or moderately faulty or severely faulty.

7.3. Arrangement of leakage faulty pistons

Further, in this section, the alternative configurations are determined for defective piston positions in such a manner to generate the least amount of peak-to-peak pressure fluctuations, and further, these configurations are classified as; the **worst (W), intermediate (R), and best (B)** corresponds to each defective piston severity (N = 1 to 9). As a result, the many damaged pistons are moved to provide the most uniform pressure distribution with the least fluctuations for optimal axial piston pump performance. The conclusion of the study carried out as follows:

1. When two defective pistons (N = 2) are identified, the alternative configuration is one with the defective pistons arranged on diametrically opposite ends or $\emptyset = 1$ for $L_s \approx L_{max}$.

2. When three or more defective pistons ($N \geq 3$) are identified, a geometrical area is described to plot a polygon (as shown in Fig. A.1) which is obtained after joining the vertex of each defective piston.

3. The alternative configuration for defective pistons (shown in Fig. 5.8) is one with the maximum geometrical area enclosed ($\emptyset \rightarrow \max$), and the optimized performance of the axial piston pump is selected based on the least amount of peak-to-peak pressure fluctuations, and the least vibrational effects, which results in the most dynamically balanced configuration for an axial piston pump.

Moreover, the position of healthy and defective pistons inside the axial piston pump is detected by a plurality of pressure/flow sensors. After repositioning the defective pistons inside the axial piston pump for uniform pressure distribution, the performance of the axial piston pump is optimized. And the optimized performance of the axial piston pump is selected based on the least amount of peak-to-peak pressure fluctuations and the least vibrational effects to classify the defective pistons from the healthy pistons. The present study can assist in anticipating the pump's health and layout preventive ways of monitoring the pump's performance to reduce its unplanned downtime. Further, the industries might reuse these defective pumps for an extended period. Because of this, they will be able to make the most of the pump's life and use it to its maximum effectiveness, reducing maintenance costs even when utilizing old and defective pumps. The hydraulic industry can benefit from this technique in cost and reusability.

7.4. Summary

According to the findings of the leakage study of an axial piston pump done in this thesis, the entire performance of an APP is strongly affected by three parameters: **Leakage severity** (h), **Piston fault severity** (N), and faulty **pistons configuration or position** ($\emptyset$) within a barrel.

The present research study can assist in anticipating the pump's health and layout preventive ways of monitoring the pump's performance to reduce its unplanned downtime. Further, the industries might reuse these defective pumps for an extended period. Because of this, they will be able to use it to its maximum effectiveness and reduce maintenance costs even when utilizing old and defective pumps. The hydraulic industry can benefit from this technique in cost and reusability.

7.5. Recommendations for future work

1. Firstly, the leakage flow past the piston-cylinder clearance in an APP may not occur due to just one factor, such as the leakage severity or the number of faulty cylinders (as described in this study). Other factors that can induce leakage fault are eccentricity and the circumferential arrangement of faulty cylinders, whether the fault occurs due to an individual factor or by combining a few or all the factors and taking corrective action accordingly.

2. Secondly, the future work may also be dedicated to developing experimental research studies and comparing the physics-based models (mentioned in this paper) that may help in leaking fault detection while accounting for all parameters such as the degree of wear, the amount of eccentricity, the number of faulty cylinders, and their different arrangements.

APPENDIX-A

Derivation of configuration ratio (CR)

In reference to Fig. A.1, for a different degree of piston fault severity, the value of A_S and L_S is changing and the A_C constant corresponds to different faults, and $\emptyset$ the value always lies between 0 and 1. To calculate the required areas of each mentioned shaded and face areas as shown in equations where $m, n \in (1\ to\ 9)$ in Eq. A1 – A7:

A_t: area of each Sub-divided triangle with defective pistons as the vertices = area $|\Delta\ OP_iP_j|$

A_S: Total area of all sub triangles (Shaded area, irregular closed polygon) = $\sum_{i,j} A_t$

A_C: Total cylindrical face area $= \pi R^2$,

R: pitch circle radii of barrel

Figure A.1 starts from one defective piston's vertex and walks around the next defective piston clockwise. Assume the center of each defective piston as vertices $(X_i, Y_i)\ \forall\ i, j \in$ (1 to 9) of the irregular polygon (nonuniform defective piston distribution). The area of the n-sided irregular closed polygon is calculated by using the equations:

- $$A_t = \frac{1}{2} \cdot \begin{vmatrix} i & j & k \\ X_i & Y_i & 0 \\ X_{i+1} & Y_{i+1} & 0 \end{vmatrix} \tag{A1}$$

- $$A_t = \frac{1}{2} \cdot |X_i \cdot Y_{i+1} - X_{i+1} \cdot Y_i|\ \ \forall\ i \in m, n \tag{A2}$$

- $$X_i = R \cdot cos\left(\frac{2\pi}{N}\right) \tag{A3}$$

- $Y_i = R \cdot sin\,(\frac{2\pi}{N})$ (A4)

N: Total number of pistons in axial piston pump

- $A_S = \sum_{i,j} A_t$ (A5)

- $A_C = \pi R^2$ (A6)

- $Configuration\ ratio\ (CR);\ \emptyset = \left(\frac{A_S}{A_c}\right) or \left(\frac{L_S}{L_{max}}\right)$ (A7)

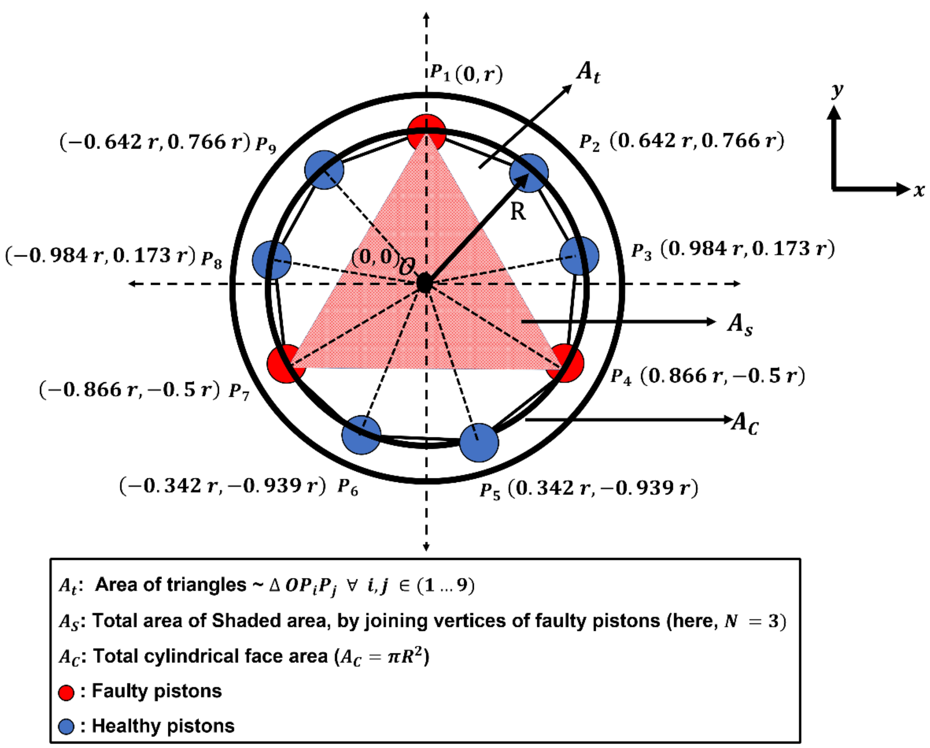

Fig. A.1: Cross-sectional view of cylinder barrel of APP with all 9 pistons arrangements. Each vertex of the triangle is considered the center of a piston; $\boldsymbol{P_1}$ ***to*** $\boldsymbol{P_9}$ Coordinates (X, Y) respectively, and **O** (0,0) act as a center of origin of whole circular geometry.

REFERENCES

[1] Pumps, Valves & Accessories Articles on Thomasnet. Reference to a website: https://www.thomasnet.com/articles/pumps-valves-accessories/. [Retrieved 26 May 2021].

[2] Haynes JM, Axial Piston Pump Leakage Modelling and Measurement, The University of Cardiff, Nov. Reference to a website: (2007). http://orca.cf.ac.uk/55178/1/U585568,

[3] Lasaar, R. The influence of the microscopic and macroscopic gap geometry on the energy dissipation in the lubricating gaps of displacement machines. *1st Fluid Power Net International PhD Symposium, pp*. 101-116 Hamburg, (2000).

[4] Lasaar, R. and Ivantysynova, M. Gap geometry variations in displacement machines and their effect on the energy dissipation. *International Conference Fluid Power Transmission and Control pp*. 296-301 Hangzhou, China, (2001).

[5] Ivantysynova M, Lasaar R. An investigation into micro-and macrogeometric design of m-piston/cylinder assembly of swash plate machines. Vol. 5, (2004).

[6] Tang H, Yang W, Wang Z. A model-based method for leakage detection of piston pump under variable load condition. *IEEE Access*; 7:99771–81, (2019). https://doi.org/10.1109/ACCESS.2019.2930816.

[7] Li Z. Condition Monitoring of Axial Piston Pump. n.d. (2005). https://harvest.usask.ca/handle/10388/etd-11252005-202705,

[8] Kumar N, Sarkar BK, Maity S. Leakage based condition monitoring and pressure control of the swashplate axial piston pump. *ASME Gas Turbine India Conference, GTINDIA, vol. 2, American Society of*

Mechanical Engineers (ASME); (2019). https://doi.org/10.1115/GTINDIA2019-2385.

[9] Zhang C, Huang S, Du J, Wang X, Wang S, Zhang H. A new dynamic seven-stage model for thickness prediction of the film between valve plate and cylinder block in axial piston pumps. *Advances in Mechanical Engineering*; 8:1–15. (2016). https://doi.org/10.1177/1687814016671446.

[10] Bergada JM, Kumar S, Davies DL, Watton J. A complete analysis of axial piston pump leakage and output flow ripples. *Applied Mathematical Modelling*; 36:1731–51. (2012). https://doi.org/10.1016/j.apm.2011.09.016,

[11] Prakash, Jatin, P. K. Kankar, and Ankur Miglani. "Monitoring the degradation in the switching behavior of a hydraulic valve using recurrence quantification analysis and fractal dimensions." *Journal of Computing and Information Science in Engineering 21.6*: 061010. (2021). https://doi.org/10.1115/1.4050821.

[12] Wang S, Xiang J. A minimum entropy deconvolution-enhanced convolutional neural networks for fault diagnosis of axial piston pumps. *Soft Computing*; 24:2983–97. (2020). https://doi.org/10.1007/s00500-019-04076-2,

[13] Wang S, Xiang J, Zhong Y, Tang H. A data indicator-based deep belief networks to detect multiple faults in axial piston pumps. *Mechanical Systems and Signal Processing* ; 112:154–70. (2018). https://doi.org/10.1016/j.ymssp.2018.04.038.

[14] Yoder VA, Singh R, Dreyer JT, Lilly B. Development of a Vibration-Based Health Monitoring Procedure using a Virtual Axial Piston Pump. (2015). http://hdl.handle.net/1811/86176,

[15] Chen, H., Chua, P., & Lim, G. Dynamic vibration analysis of a swash-plate type water hydraulic motor. *Mechanism And Machine Theory, 41(5), 487-504.* (2006). doi: 10.1016/j.mechmachtheory.2005.09.002.

[16] Casoli P, Pastori M, Scolari F, Rundo M. A vibration signal-based method for fault identification and classification in hydraulic axial piston pumps. *Energies*; 12. (2019). https://doi.org/10.3390/en12050953.

[17] Prakash J, Kankar PK. Health prediction of hydraulic cooling circuit using deep neural network with ensemble feature ranking technique. *Measurement: Journal of the International Measurement Confederation*;151. (2020). https://doi.org/10.1016/j.measurement.2019.107225.

[18] Prakash, Jatin, Sumit Kumar Gupta, and P. K. Kankar. "An analytical approach to evaluate the maximum load carrying capacity for pin-mounted telescopic hydraulic cylinder." *Proceedings of the Institution of Mechanical Engineers, Part C: Journal of Mechanical Engineering Science 234, no. 19: 3919-3934.* (2020).

[19] Prakash, Jatin, and P. K. Kankar. "Determining the working behaviour of hydraulic system using support vector machine". *Lecture Notes in Mechanical Engineering, 781-791.* (2021). doi:10.1007/978-981-15-8025-3_74.

[20] Yin F, Nie S, Hou W, Xiao S. Effect analysis of silencing grooves on pressure and vibration characteristics of seawater axial piston pump. *Proceedings of the Institution of Mechanical Engineers, Part C: Journal of Mechanical Engineering Science*; 231:1390–409. (2017). https://doi.org/10.1177/0954406216660334.

[21] Kumar S, Bergada JM. The effect of piston grooves performance in an axial piston pump via CFD analysis. *International Journal of*

Mechanical Sciences; 66:168–79. (2013). https://doi.org/10.1016/j.ijmecsci.2012.11.005.

[22] Pijush K. Kundu, Ira M. Cohen and David R. Dowling. 5th ed. Fluid Mechanics, ScienceDirect. https://doi.org/10.1016/C2009-0-63410-3 (2012). Reference to a website: https://www.sciencedirect.com/book/9780123821003/fluid- mechanics #book-description. [Retrieved 26 May 2021]

[23] White, Frank M. Fluid mechanics, 4th ed. McGraw hill; (1986). Reference to a website: http://vlib.kmu.ac.ir/kmu/handle/kmu/80712.

[24] Ivantysyn, J and Ivantysynova, M Hydrostatic Pumps and Motors, Akademia *Books International Publishers & Distributor, New Delhi, India*. (2001). Reference to a website: https://engineering.purdue.edu/Maha/publications_ivantysynova.

[25] PVM Piston Pumps Service Manual, Reference to a website: https://www.eaton.com/ecm/groups/public/pub/@eaton/@hyd/documents/content/pct_477093.pdf. [Retrieved 26 May 2021].

[26] Vickers Industrial Hydraulics Manual Reference to a website: https://fdocuments.in/document/289203703-vickers-industrial-hydraulics-manual.html. (2021), [Retrieved 26 May 2021].

[27] Hydraulic Axial Piston Eaton Vickers PVB Pump, Reference to a website; http://www.hydpump.com/pdf/Vickers%20PVB%20MVB%20piston%20pump.pd. [Retrieved 26 May 2021].

[28] Zhang, J., Chao, Q., Xu, B., Pan, M., Wang, Q., & Chen, Y. Novel three-piston pump design for a slipper test rig. *Applied Mathematical Modelling, 52, 65-81*. (2017). doi: 10.1016/j.apm.2017.07.013.

[29] Lyu, Fei, Shaogan Ye, Junhui Zhang, Bing Xu, Weidi Huang, Haogong Xu, and Xiaochen Huang. "Theoretical and simulation investigations on flow ripple reduction of axial piston pumps using nonuniform distribution of pistons". *J Dyn Syst-T ASME* 143 (4). (2020). doi:10.1115/1.4048859.

[30] Roccatello, Alessandro, Salvatore Mancò, and Nicola Nervegna. "Modelling a variable displacement axial piston pump in a multibody simulation environment". *J Dyn Syst-T ASME* 129 (4): 456-468. (2006). doi:10.1115/1.2745851.

[31] Manring, Noah D. "The discharge flow ripple of an axial-piston swash-plate type hydrostatic pump". *Journal Of Dynamic Systems, Measurement, And Control* 122 (2): 263-268. (1998). doi:10.1115/1.482452.

[32] Edge, K. A., and J. Darling. "The pumping dynamics of swash plate piston pumps". *J Dyn Syst-T ASME* 111 (2): 307-312. (1989). doi:10.1115/1.3153051.

[33] Schoenau, G. J., R. T. Burton, and G. P. Kavanagh. "Dynamic analysis of a variable displacement pump". *J Dyn Syst-T ASME* 112 (1): 122-132. (1990). doi:10.1115/1.2894129.

[34] Manring, N. D., and R. E. Johnson. "Modeling and Designing A Variable-Displacement Open-Loop Pump *J Dyn Syst-T ASME* 118 (2): 267-271. (1996). doi:10.1115/1.2802313.

[35] Ranawat NS, Kankar PK., and Miglani Ankur. "Fault diagnosis in centrifugal pump using support vector machine and artificial neural network ". *Journal of Engineering Research- EMSME Special Issue pp. 99-111*. (2020). doi: https://doi.org/10.36909/jer.EMSME.13881.

[36] Zhang, X., J. Cho, S. S. Nair, and N. D. Manring. "New swash plate damping model for hydraulic axial-piston pump". *Journal Of Dynamic*

Systems, Measurement, And Control 123 (3): 463-470. (1999). doi:10.1115/1.1386789.

[37] M. Pelosi and M. Ivantysynova, "The impact of axial piston machines mechanical parts constraint conditions on the thermo-electrohydrodynamic lubrication analysis of the fluid film interfaces," *International Journal of Fluid Power*, vol. 14, no. 3, pp. 35–51, (2013). doi: 10.1080/14399776.2013.10801412.

[38] M. Z. Norhirni, M. Hamdi, S. Nurmaya Musa, L. H. Saw, N. A. Mardi, and N. Hilman, "Load and stress analysis for the swash plate of an axial piston pump/motor," *Journal of Dynamic Systems, Measurement, and Control, Transactions of the ASME*, vol. 133, no. 6, (2011). doi: 10.1115/1.4004578.

[39] J. H. Shin, "Computational study on dynamic pressure in a swashplate axial piston pump connected to a hydraulic line with an end resistance," *Journal of Mechanical Science and Technology*, vol. 29, no. 6, pp. 2381–2390, Jun. (2015). doi: 10.1007/s12206-015-0531-1.

[40] Ivantysynova, Monika Prof. and Changchun Huang. “Investigation of the gap flow in displacement machines considering electrohydrodynamic effect.” (2002).

[41] J. M. Bergada, D. L. Davies, S. Kumar, and J. Watton, "The effect of oil pressure and temperature on barrel film thickness and barrel dynamics of an axial piston pump," *Meccanica*, vol. 47, no. 3, pp. 639–654, (2012), doi: 10.1007/s11012-011-9472-7.

[42] R. Klop and M. Ivantysynova, "Investigation of noise sources on a series hybrid transmission," *International Journal of Fluid Power*, vol. 12, no. 3, pp. 17–30, (2011), doi: 10.1080/14399776.2011.10781034.

[43] G. Kumar Seeniraj and M. Ivantysynova, "A multi-parameter multi-objective approach to reduce pump noise generation," *International*

Journal of Fluid Power, vol. 12, no. 1, pp. 7–17, (2011), doi: 10.1080/14399776.2011.10781018.

[44] Fang, Yi, and Masataka Shirakashi. "Mixed lubrication characteristics between the piston and cylinder in hydraulic piston pump-motor". *Journal Of Tribology 117 (1): 80-85*. (1995), doi:10.1115/1.2830610.

[45] Manring, Noah D. "Friction forces within the cylinder bores of swash-plate type axial-piston pumps and motors". *Journal Of Dynamic Systems, Measurement, And Control 121 (3): 531-537*. (1999). doi:10.1115/1.2802507.

[46] M. Pelosi and M. Ivantysynova, "A novel thermal model for the piston/cylinder interface of piston machines," (2009). Available: http://www.asme.org/about-asme/terms-of-use.

[47] Pelosi, M, & Ivantysynova, M. "Surface Deformations Enable High Pressure Operation of Axial Piston Pumps.*" Proceedings of the ASME 2011 Dynamic Systems and Control Conference and Bath/ASME Symposium on Fluid Power and Motion Control. ASME 2011 Dynamic Systems and Control Conference and Bath/ASME Symposium on Fluid Power and Motion Control, Volume 1. Arlington, Virginia, USA*. October 31–November 2, (2011). pp. 193-200. ASME. https://doi.org/10.1115/DSCC2011-5979

[48] M. Pelosi and M. Ivantysynova, "A geometric multigrid solver for the piston-cylinder interface of axial piston machines," *Tribology Transactions*, vol. 55, no. 2, pp. 163–174, Mar. (2012), doi: 10.1080/10402004.2011.639049.

[49] M. Pelosi and M. Ivantysynova, "Heat transfer and thermal elastic deformation analysis on the Piston/Cylinder interface of axial piston machines," *Journal of Tribology*, vol. 134, no. 4, (2012), doi: 10.1115/1.4006980.

[50] Łatas W, Stojek J. Dynamic model of axial piston swashplate pump for diagnostics of wear in elements. *Archive of Mechanical Engineering;58:135–55*. (2011). https://doi.org/10.2478/v10180-011-0010-x.

[51] Pumps, Valves & Accessories Articles on Thomasnet. Reference to a website: https://www.thomasnet.com/articles/pumps-valves-accessories/. [Retrieved 26 May 2021].

[52] Bhupendra, Kriz Moses, Ankur Miglani, and Pavan Kumar Kankar. "Deep CNN-based damage classification of milled rice grains using a high-magnification image dataset". *Computers and Electronics in Agriculture*, vol. 195: 106811. (2022). doi: 10.1016/j.compag.2022.106811.